Brazilian Journal of Physics (2025) 55:135
https://doi.org/10.1007/s13538-025-01769-y

On the Dynamics of COVID-19 Propagation with Vaccination and Optimal Control Strategies

Padma Bhushan Borah[1,2] · Dipika Robidas[3] · Kaushik Dehingia[4,5,6] · Bhagya Jyoti Nath[7] · Hemanta Kumar Sarmah[1]

Received: 21 February 2025 / Accepted: 4 April 2025 / Published online: 15 April 2025
© The Author(s) 2025

Abstract

In this paper, a mathematical model is proposed to describe the spread dynamics of COVID-19, considering the factors of self-protection and vaccination. The basic reproduction number of the model, which is a critical signal of the dynamics of COVID-19 transmission, is calculated using the next-generation matrix method. A study of the local stability of steady states has been conducted. Moreover, global stability is demonstrated using Lyapunov's second method and LaSalle's invariance principle. In addition, the effect of vaccination on the evolution of the disease spread has been studied. Further, an optimal control problem is formulated and solved to reduce the number of infected individuals and the cost of the controls by considering self-protection and vaccination as intervention options. Specifically, our results indicate that implementing optimal control strategies, such as time-dependent interventions, reduces disease transmission and overall infection burden. The model demonstrates that strategically timed and intensity-optimized control measures can flatten the epidemic curve, delay peak infection, and minimize the outbreak's cost and duration. Finally, comprehensive simulations were performed across various initial conditions and parameter settings to verify the theoretical findings.

Keywords COVID-19 pandemic · Stability · Basic reproduction number · Vaccination · Optimal control · Pontryagin maximum principle · Numerical simulations

1 Introduction

The coronavirus disease (COVID-19) was first observed in December 2019 in the Wuhan Province of China, and then it spread throughout the world. It affected the whole world in the most devastating way possible. The World Health Organization (WHO) officially declared COVID-19 a global pandemic on March 11, 2020. The predominant route of COVID-19 transmission occurs via direct contact with an individual carrying the infection. Globally, COVID-19 has infected over 600 million individuals, resulting in more than 6 million fatalities [1–3]. In addition to a lack of diagnostics, many cases are asymptomatic, contributing to the underestimation of instances [4–7]. China's Wuhan, Hubei, was the first place to detect COVID-19 [8–12]. Afterward, nearly every country was affected by the virus.

The tremendous efforts of numerous scientists have led to the advancement of vaccines for COVID-19 like the Pfizer/BioNTech Comirnaty vaccine, the Bharat Biotech BBV152 COVAXIN vaccine, the COVISHIELD vaccine, and the AstraZeneca/AZD1222 vaccine [3, 13]. While most vaccines need two doses, Johnson & Johnson requires only one [13, 14]. It is almost impossible to vaccinate all susceptible persons, mainly due to economic reasons. This is especially so in nations where vaccines are difficult to get

✉ Kaushik Dehingia
kaushikdehingia17@gmail.com

1 Department of Mathematics, Gauhati University, Guwahati 781014, India

2 Department of Mathematics, Cotton University, Guwahati, Assam 781001, India

3 Department of Physics, North Lakhimpur University, Lakhimpur, Assam 787031, India

4 Department of Mathematics, Sonari College, Sonari, Assam 785690, India

5 Research Center of Applied Mathematics, Khazar University, Baku, Azerbaijan

6 Mathematics Research Center, Near East University, Nicosia 99318, Turkey

7 Department of Mathematics, Rabindranath Tagore University, Hojai, Assam 782435, India

or prohibitively expensive. Consequently, the building of a framework capable of predicting the optimal level of vaccine coverage is a top priority for health administrators and policymakers.

Epidemiological modeling has significantly advanced the comprehension of the propagation patterns of infectious diseases, which is essential for implementing effective control measures [15–23]. The investigation of smallpox transmission dynamics in 1760 initiated the exploration of epidemic modeling, which has progressively developed into a crucial framework for analyzing the spread of pandemics [24]. Kermack and McKendrick [25] developed a mathematical model characterized by three ordinary differential equations, which are widely recognized as the susceptible-infected-removed (SIR) model for infectious diseases. In a typical SIR model, the total population is divided into three categories: susceptible individuals $S(t)$, infected individuals $I(t)$, and removed individuals (either through recovery or death) $R(t)$ [25, 26]. However, a latent phase precedes the development of many infectious diseases. This necessitates the addition of an additional compartment $E(t)$ representing the exposed population to the model, leading to a system of four ordinary differential equations (ODEs) [27]. In [28], an extended SIR model has been developed by adding the exposed class $E(t)$. Bailey and Bartlett [29, 30] pioneered the development of stochastic models to describe infectious disease transmission dynamics in the 1950s and early 1960s. Moreover, Bartlett was the first to use the Monte Carlo simulation technique to study epidemics of contagious diseases [31, 32].

Since the outbreak of COVID-19, a significant number of researchers have passionately contributed to enhancing epidemiological modeling [33–42]. The SEIR model has been employed during the COVID-19 outbreak to understand the initial dynamics and evaluate the effectiveness of interventions implemented following the outbreak [43–47]. In [48], a fractional modeling study has been carried out to investigate the transmission mechanism of SARS-CoV-2, taking into account the different phases of infection and transmission routes. Also, Zarin et al. [49] discussed a reaction-diffusion framework to understand the spread of the disease so that effective public health intervention strategies can be taken. A study on the co-dynamics of monkeypox and COVID-19 diseases has been conducted in [50] to understand the impact of robust control measures and the fractal dimension. The idea of optimal control procedure has been utilized in the study of COVID-19 transmission in [51–53], demonstrating that optimal control strategies can effectively mitigate the spread of the novel coronavirus.

In this study, we introduce a compartment-based model [54] that includes the class $V(t)$ representing vaccinated individuals and the class $P(t)$ representing self-protected individuals. The $P(t)$ compartment reflects the behavioral response of individuals who adopt protective measures (e.g., mask-wearing, hand hygiene, avoiding crowds) without being infected, exposed, or vaccinated. Unlike traditional SEIRV models, which typically assume homogeneous mixing and overlook individual-level behavior modification, our model explicitly accounts for a dynamic subgroup of the population that alters its risk profile through self-initiated protection. This compartment not only reduces the effective contact rate but also influences the overall transmission dynamics by creating a feedback loop between public perception and disease spread. Incorporating this behavioral dimension improves the realism and predictive power of the model, especially in scenarios where public awareness and compliance significantly affect epidemic outcomes. As shown in [55], COVID-19 cannot be adequately characterized by deterministic models with fewer than five compartments, such as SIR and SEIR. This research seeks to investigate the transmission dynamics of the COVID-19 epidemic by employing the PSEIRV model in combination with the principles of dynamical system theory. While the discrete model offers comparable accuracy, we focus on the continuous deterministic model due to its simplicity in analysis. Additionally, we will assess the influence of vaccination on the dynamics of the model.

In addition, by incorporating self-protection and vaccination as control strategies, a problem in optimal control is formulated for the proposed model, and the corresponding optimal control solution is systematically characterized. Unlike previous epidemic control models that often assume static or uniform intervention strategies, our model incorporates a time-dependent optimal control framework that dynamically adjusts intervention levels based on the current epidemic state. This allows for a more realistic and efficient allocation of resources. Furthermore, our model integrates multiple control variables simultaneously (e.g., vaccination and public awareness), capturing the synergistic effects of combined strategies. We also account for constraints such as limited resources or behavioral responses, which are often overlooked in classical models. These enhancements provide a more robust and adaptable framework for informing public health decision-making.

The rest of the paper is amended as follows: In Sect. 2, the model formulation is described. Section 3 presents the essential characteristics of the model, including positivity, boundedness, and the region of invariance. Section 4 determines the disease-free equilibrium and the basic reproduction number. Section 5 focuses on determining the endemic equilibrium of the model. Section 6 examines the impact of vaccination, while Sect. 7 dealt with the model's stability. In Sect. 8, the existence of optimal control in terms of the self-protection rate and vaccination rate that optimally reduces the disease is investigated. In Sect. 9, a few numerical examples are performed to validate the conclusions drawn in the pre-

vious sections. The conclusion and discussion are contained in the final Sect. 10.

2 Model Formulation

Here, we designed a compartment-based model to illustrate the spread of COVID-19. The model classifies the entire population into six crucial subgroups: the susceptible class $S(t)$, people who can potentially get COVID-19; self-protected class $P(t)$, these are the people adhering to protective measures like wearing masks, social distancing, sanitizing, etc., and hence insusceptible to infection; those in the latent phase of infection $L(t)$, these are the people who are infected but not yet infectious; those who are infectious $I(t)$, they are the ones spreading the infection; those who have been vaccinated $V(t)$, and the survivors of COVID-19 $R(t)$. Each compartment is presumed to be homogeneous. Consequently, everyone in the same compartment faces the same hazards. It is also assumed that a person develops immunity after recovering from the illness. Furthermore, all newborns are considered vulnerable to infection. The total population can be determined as

$$N(t) = P(t) + V(t) + S(t) + L(t) + I(t) + R(t),$$

at any time t. We have developed the following model based on the above assumptions:

$$\begin{cases} \frac{dP(t)}{dt} = pS - dP, \\ \frac{dS(t)}{dt} = b - \beta IS - (d + v + p)S, \\ \frac{dL(t)}{dt} = \beta IS - (d + \sigma)L, \\ \frac{dI(t)}{dt} = \sigma L - (d + \gamma)I, \\ \frac{dR(t)}{dt} = \gamma I - dR, \\ \frac{dV(t)}{dt} = vS - dV, \end{cases} \tag{1}$$

with the initial conditions

$$P(0) \geq 0, S(0) \geq 0, L(0) \geq 0, I(0) \geq 0,$$
$$R(0) \geq 0, V(0) \geq 0. \tag{2}$$

Here, the constant birth rate and the natural death rate are denoted by b and d, respectively, whereas β denotes the effective contact rate of the susceptible population with the infectious population, and p denotes the protection rate. The rate of vaccination is denoted by v. σ represents the rate at which the exposed class transitions to the infectious class, and γ is the natural recovery rate. Figure 1 depicts the mathematical model as a diagram (1).

3 Basic Properties

From the perspective of biological scenarios, the solution of the system (1) must be positive and bounded in the region $\mathbb{R}^6_+$. Thus, this section will examine the primary characteristic of the solutions of the system (1) with the initial conditions (2) such as positivity and boundedness.

Theorem 1 *Suppose the parameters and initial values are positive. In that case, for all time t, the solutions of the system (1), i.e., $P(t)$, $V(t)$, $S(t)$, $L(t)$, $I(t)$, and $R(t)$, remain positive.*

Proof We shall prove by contradiction. Let

$$\tau = \sup\{\psi > 0 | \forall t \in [0, \psi], P(t) > 0, V(t) > 0,$$
$$S(t) > 0, L(t) > 0, I(t) > 0, R(t) > 0\}.$$

By continuity of solutions $\tau > 0$ if $P(0) > 0, V(0) > 0, S(0) > 0, L(0) > 0, I(0) > 0, R(0) > 0$. Therefore, it is sufficient to show that $\tau = +\infty$.

If possible, suppose $\tau < \infty$. As a result, the continuity of solutions implies that

$$P(\tau) = 0, \text{ or } S(\tau) = 0, \text{ or } L(\tau) = 0, \text{ or } I(\tau) = 0, \text{ or}$$
$$R(\tau) = 0, \text{ or } V(\tau) = 0.$$

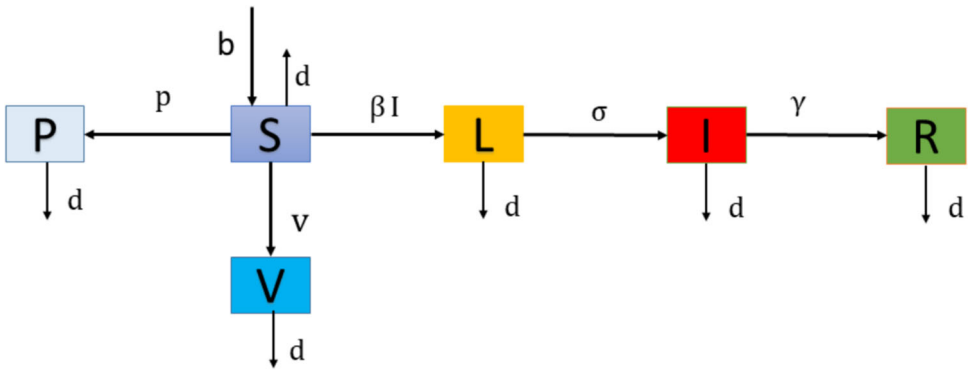


Fig. 1 Graphical presentation of the model (1)

If $P(\tau)$ is zero before the other variables become zero, then

$$\frac{dP(t)}{dt}\Big|_{t=\tau} = \lim_{t\to\tau^-}\frac{P(\tau)-P(t)}{\tau-t} = -\lim_{t\to\tau^-}\frac{P(t)}{\tau-t} \le 0. \tag{3}$$

But, the first equation of the system of equations (1) implies that

$$\frac{dP(t)}{dt}\Big|_{t=\tau} = pS(\tau) - dP(\tau) = p > 0,$$

which contradicts inequality (3).

Now, if $S(\tau) = 0$ before the other variables become zero, then

$$\frac{dS(t)}{dt}\Big|_{t=\tau} = \lim_{t\to\tau^-}\frac{S(\tau)-S(t)}{\tau-t} = -\lim_{t\to\tau^-}\frac{S(t)}{\tau-t} \le 0. \tag{4}$$

However, the second equation of (1) implies that

$$\frac{dS(t)}{dt}\Big|_{t=\tau} = b-\beta I(\tau)S(\tau)/N-(d+v+p)S(\tau) = b > 0,$$

contradicting inequality (4).

Similarly, if $L(\tau)$ becomes zero first, then

$$\frac{dL(t)}{dt}\Big|_{t=\tau} = \lim_{t\to\tau^-}\frac{L(\tau)-L(t)}{\tau-t} = -\lim_{t\to\tau^-}\frac{L(t)}{\tau-t} \le 0; \tag{5}$$

however, the third equation of (1) implies that

$$\begin{aligned}\frac{dL(t)}{dt}\Big|_{t=\tau} &= \beta I(\tau)S(\tau)/N - (d+\sigma)L(\tau)\\ &= \beta I(\tau)S(\tau)/N > 0,\end{aligned}$$

contradicting inequality (5).

Next, if $I(\tau)$ becomes zero first, then

$$\frac{dI(t)}{dt}\Big|_{t=\tau} = \lim_{t\to\tau^-}\frac{I(\tau)-I(t)}{\tau-t} = -\lim_{t\to\tau^-}\frac{I(t)}{\tau-t} \le 0, \tag{6}$$

but fourth equation of (1) gives us

$$\begin{aligned}\frac{dI(t)}{dt}\Big|_{t=\tau} &= \sigma L(\tau) - (d+\gamma)I(\tau)\\ &= \sigma L(\tau) > 0,\end{aligned}$$

contradicting inequality (6).

Again, if $R(\tau)$ becomes zero first, then

$$\frac{dR(t)}{dt}\Big|_{t=\tau} = \lim_{t\to\tau^-}\frac{R(\tau)-R(t)}{\tau-t} = -\lim_{t\to\tau^-}\frac{R(t)}{\tau-t} \le 0, \tag{7}$$

but the fifth equation of (1) gives

$$\begin{aligned}\frac{dR(t)}{dt}\Big|_{t=\tau} &= \gamma I(\tau) - dR(\tau)\\ &= \gamma I(\tau) > 0,\end{aligned}$$

contradicting inequality (7).

Lastly, if $V(\tau)$ becomes zero first, then

$$\frac{dV(t)}{dt}\Big|_{t=\tau} = \lim_{t\to\tau^-}\frac{V(\tau)-V(t)}{\tau-t} = -\lim_{t\to\tau^-}\frac{V(t)}{\tau-t} \le 0, \tag{8}$$

but the last equation of (1) implies

$$\begin{aligned}\frac{dV(t)}{dt}\Big|_{t=\tau} &= vS(\tau) - dV(\tau)\\ &= vS(\tau) > 0,\end{aligned}$$

contradicting inequality (8).

Hence, τ is infinite, proving the claim.

Therefore, all the solutions $P(t)$, $V(t)$, $S(t)$, $L(t)$, $I(t)$, and $R(t)$ of the model (1) remain positive for all $t \ge 0$ if all the parameters as well as the initial conditions are positive. Thus, Theorem 1 holds. □

Theorem 2 *Every feasible solution of the system* (1) *is bounded uniformly On* $[0, \infty)$.

Proof We add all the equations of (1) and get

$$\frac{dN(t)}{dt} + dN(t) = b. \tag{9}$$

Solving the first-order and first-degree ordinary differential equation (9), we have

$$N(t) = \left(-\frac{b}{d} + N(0)\right)e^{-dt} + \frac{b}{d}, \tag{10}$$

where $N(0)$ represents the total initial population. Equation (10) implies

$$\lim_{t\to\infty} N(t) = \frac{b}{d}, \tag{11}$$

i.e., $N(t)$ approaches $\frac{b}{d}$ asymptotically. Since $N(t) = P(t)+V(t)+S(t)+L(t)+I(t)+R(t)$ for all t, together with Theorem 1, we get all solutions of system (1) are uniformly bounded on $\mathbb{R}^+$. □

Theorem 3 *The following is a positively invariant region of model* (1)*:*

$$\Delta = \Big\{(P(t), V(t), S(t), L(t), I(t), R(t)) \in \mathbb{R}^6_+ : 0 \le S(t)$$

$$\leq \frac{b}{d+v+p}, 0 \leq N(t) \leq \frac{b}{d}\Bigg\}. \tag{12}$$

Proof From the second equation of (1), we get

$$\frac{dS(t)}{dt} \leq b - (d+v+p)S(t). \tag{13}$$

Now, applying Gronwall's inequality [56] to (13), we get

$$S(t) \leq \frac{b}{d+v+p} + \left(S(0) - \frac{b}{d+v+p}\right) e^{-(d+v+p)t}, \tag{14}$$

where $S(0)$ is the initial susceptible population. Hence, we have from (14)

$$S(0) \leq \frac{b}{d+v+p} \implies S(t) \leq \frac{b}{d+v+p} \text{ for all time } t. \tag{15}$$

Again, from (10), we obtain

$$N(0) \leq \frac{b}{d} \implies N(t) \leq \frac{b}{d} \text{ for all time } t. \tag{16}$$

By (15) and (16), the theorem follows. □

Observations From inequality (14), we have

$$\limsup_{t\to+\infty} S(t) \leq \frac{b}{d+v+p}. \tag{17}$$

So, if $S(0) > \frac{b}{d+v+p}$, then either $S(t)$ enters Δ and hence remains there thereafter, or approaches $\frac{b}{d+v+p}$ asymptotically. Similarly, by (11), if $N(0) > \frac{b}{d}$, then either $N(t)$ enters Δ and hence remains there thereafter, or asymptotically approaches $\frac{b}{d}$.

Remark In light of Theorem 1, 2, 3, and the above *observavations*, we only focus on the region Δ given by (12) to analyze the dynamics of model (1).

4 Disease-Free Equilibrium and the Basic Reproduction Number

4.1 The Disease-Free Equilibrium

We determine the equilibria of the proposed model (1) by equating the time derivatives in (1) to zero. The disease-free equilibrium $\mathscr{E}_0$ corresponds to when $I = 0$, i.e., no infection. Solving (1) for $I = 0$ and $\dot{P} = \dot{V} = \dot{S} = \dot{L} = \dot{I} = \dot{R} = 0$ gives us the following unique disease-free equilibrium:

$$\mathscr{E}_0 = (P_0, V_0, S_0, L_0, I_0, R_0) = \left(\frac{pb}{d(d+v+p)}, \frac{b}{d+v+p}, 0, 0, 0, \frac{vb}{d(d+v+p)}\right). \tag{18}$$

4.2 Basic Reproduction Number (BRN) $\mathscr{R}_0$

The *BRN*, denoted by $\mathscr{R}_0$, is the "expected number of secondary cases that would arise from a typical primary case in a completely susceptible population" [57–61]. $\mathscr{R}_0$ [58–61] reflects an infection's severity. The formula for the basic reproduction number of model (1) will be derived using the next-generation matrix methods explained in [60–62]. To begin with, we find the matrices $\mathscr{F}$ and $\mathscr{W}$, where $\mathscr{F}$ represents newly arising infections and $\mathscr{W}$ represents net transitions between the infective compartments. We then compute the Jacobian matrices of $\mathscr{F}$ and $\mathscr{W}$ at the disease-free equilibrium for F and W, respectively. The basic reproduction number $\mathscr{R}_0$ then is given by $\rho(FW^{-1})$, the spectral radius of FW^{-1}.

In the following steps, we calculate the *BRN* $\mathscr{R}_0$ for the model (1) based on [57, 62]:

Step 1. There are *two* compartments that have been infected: L and I.

Step 2. New infections are represented by the 2×1 matrix $\mathscr{F}$:

$$\mathscr{F} = \begin{bmatrix} \beta IS \\ 0 \end{bmatrix}.$$

Step 3. The 2×1 matrix $\mathscr{W}^-$ that comprises terms emanating from each diseased compartment is as follows:

$$\mathscr{W}^- = \begin{bmatrix} (d+\sigma)L \\ (d+\gamma)I \end{bmatrix}.$$

Step 4. The 2×1 matrix $\mathscr{W}^+$ that contains entries entering each infected compartment except fresh infections is as follows:

$$\mathscr{W}^+ = \begin{bmatrix} 0 \\ \sigma L \end{bmatrix}.$$

Step 5. Net transfer between infected compartments, excluding fresh infections, is calculated by the 2×1 matrix $\mathscr{W} = \mathscr{W}^- - \mathscr{W}^+$:

$$\mathscr{W} = \begin{bmatrix} (d+\sigma)L \\ (d+\gamma)I - \sigma L \end{bmatrix}.$$

Step 6. At $\mathscr{E}_0$ (18), the 2×2 Jacobian matrix F of the two infectious state variables $y = [L, I]^{\mathrm{T}}$ is computed as follows:

$$\begin{aligned} F &= \left[\frac{\partial \mathscr{F}}{\partial y}\right]_{\text{at } \mathscr{E}_0} \\ &= \begin{bmatrix} 0 & \beta S_0 \\ 0 & 0 \end{bmatrix}, \\ &= \begin{bmatrix} 0 & \frac{\beta b}{d+p+v} \\ 0 & 0 \end{bmatrix}. \end{aligned}$$

Step 7. The 2×2 Jacobian matrix W that is the partial derivative of $\mathscr{W}$ w.r.t. the vector $y = [L, I]^{\mathrm{T}}$ computed at $\mathscr{E}_0$ (18) is as follows:

$$\begin{aligned} W &= \left[\frac{\partial \mathscr{W}}{\partial y}\right]_{\text{at } \mathscr{E}_0} \\ &= \begin{bmatrix} d+\sigma & 0 \\ -\sigma & d+\gamma \end{bmatrix}. \end{aligned}$$

Step 8. The inverse of W is as follows:

$$W^{-1} = \begin{bmatrix} \frac{1}{\sigma+d} & 0 \\ \frac{\sigma}{(\sigma+d)(\gamma+d)} & \frac{1}{\gamma+d} \end{bmatrix}.$$

Step 9. The next-generation matrix is as follows:

$$FW^{-1} = \begin{bmatrix} \frac{\beta b \sigma}{(d+\gamma)(d+\sigma)(d+p+v)} & \frac{b\beta}{(d+\gamma)(d+p+v)} \\ 0 & 0 \end{bmatrix}.$$

And lastly,

Step 10. The *BRN* $\mathscr{R}_0$ is determined as the biggest eigenvalue $\rho(FW^{-1})$ of FW^{-1}. Thus, we get the following:

$$\mathscr{R}_0 = \frac{b\beta\sigma}{(d+\sigma)(d+\gamma)(d+p+v)}. \tag{19}$$

5 The Endemic Equilibrium

Endemic steady-state $\mathscr{E}_1$ is attained if an infection is present, i.e., $I \neq 0$. Zeroing the right-hand side of (1) at $\mathscr{E}_1 = (P_1, V_1, S_1, L_1, I_1, R_1)$, we get

$$\begin{cases} 0 = pS_1 - dP_1, \\ 0 = b - \beta I_1 S_1 - (d+v+p)S_1, \\ 0 = \beta I_1 S_1 - (d+\sigma)L_1, \\ 0 = \sigma L_1 - (d+\gamma)I_1, \\ 0 = \gamma I_1 - dR_1, \\ 0 = vS_1 - dV_1. \end{cases} \tag{20}$$

Solving (20) and $I_1 \neq 0$ results in the following unique endemic equilibrium point $\mathscr{E}_1$:

$$\begin{cases} P_1 = \dfrac{P_0}{\mathscr{R}_0}, \\ V_1 = \dfrac{V_0}{\mathscr{R}_0}, \\ S_1 = \dfrac{S_0}{\mathscr{R}_0}, \\ L_1 = \dfrac{b}{d+\sigma}\dfrac{\mathscr{R}_0 - 1}{\mathscr{R}_0}, \\ I_1 = \dfrac{d+p+v}{\beta}(\mathscr{R}_0 - 1), \\ R_1 = \dfrac{\gamma(d+v+p)}{\beta d}(\mathscr{R}_0 - 1). \end{cases} \tag{21}$$

6 Effect of Vaccination

Vaccination plays a critical role in our model by directly removing individuals from the susceptible class and transferring them to the vaccinated compartment, thereby reducing the number of individuals who can acquire and transmit the disease. This mechanism effectively lowers the force of infection and contributes to the reduction of the basic reproduction number $\mathscr{R}_0$. Our model incorporates vaccination as both a parameter (for static analysis) and as a time-dependent control variable (in the optimal control framework). In the analytical expression for $\mathscr{R}_0$, vaccination appears in the denominator as part of the term $(d + p + v)$, which reflects the rate at which susceptibles exit due to self-protection, vaccination, or natural death. As the vaccination rate v increases, $\mathscr{R}_0$ decreases accordingly.

Let us denote the *BRN* (19) as a function of the vaccination rate v, i.e.,

$$\mathscr{R}(v) := \frac{b\beta\sigma}{(d+\sigma)(d+\gamma)(d+p+v)}. \tag{22}$$

Taking $v - derivative$ of (22), one gets

$$\mathscr{R}'(v) = -\frac{\mathscr{R}(v)}{d+p+v} < 0. \tag{23}$$

Hence, (23) implies the *BRN* $\mathscr{R}(v)$ is a decreasing function of v.

We observe that even moderate increases in the vaccination rate can lead to significant reductions in $\mathscr{R}_0$. Thus, even if $\mathscr{R}_0$ is more than 1 initially, it can be brought to a value lower than 1 by employing vaccination, thereby eradicating the infection.

Furthermore, numerical simulations reveal a threshold behavior: when vaccination coverage exceeds a certain level, the infection curve flattens dramatically and may even fail

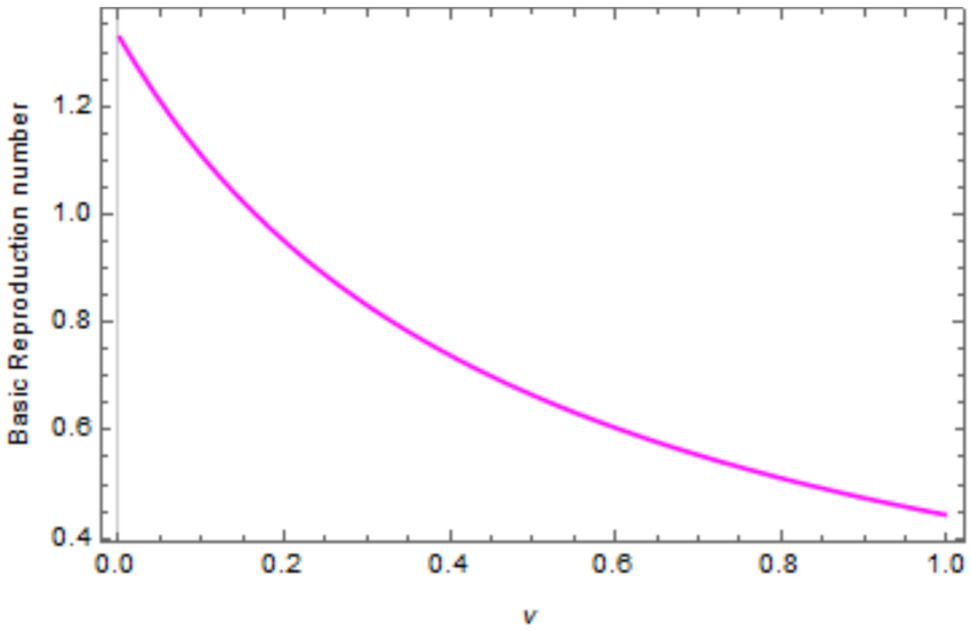


Fig. 2 Basic reproduction number vs. rate of vaccination

to reach a substantial outbreak phase. Although our current work does not define an explicit critical vaccination threshold (as in classical herd immunity formulations), our simulations and control results do indicate the existence of such practical thresholds where vaccination has a disproportionately large impact on disease control. These findings highlight the importance of timely and sufficiently high vaccination coverage as part of an integrated disease mitigation strategy. Figure 2 shows the *BRN* as a function of the vaccination rate v.

In addition, we analyze the quantitative impact of vaccination on the basic reproduction number $\mathscr{R}_0$. As shown in Fig. 3, increasing the vaccination rate v has a nonlinear suppressive effect on disease transmission. Notably, when $v \geq 0.18$, $\mathscr{R}_0$ falls below the epidemic threshold of 1. This corresponds to an approximate 26.7% reduction in $\mathscr{R}_0$ from its baseline value, indicating a critical threshold beyond which the disease cannot sustain transmission in the population.

7 Stability Analysis

Here, we examine the equilibrium points' stability derived in (1) and (21) for the model (1). We shall demonstrate that the value of $\mathscr{R}_0$ is intrinsically linked to that of steady states' stability.

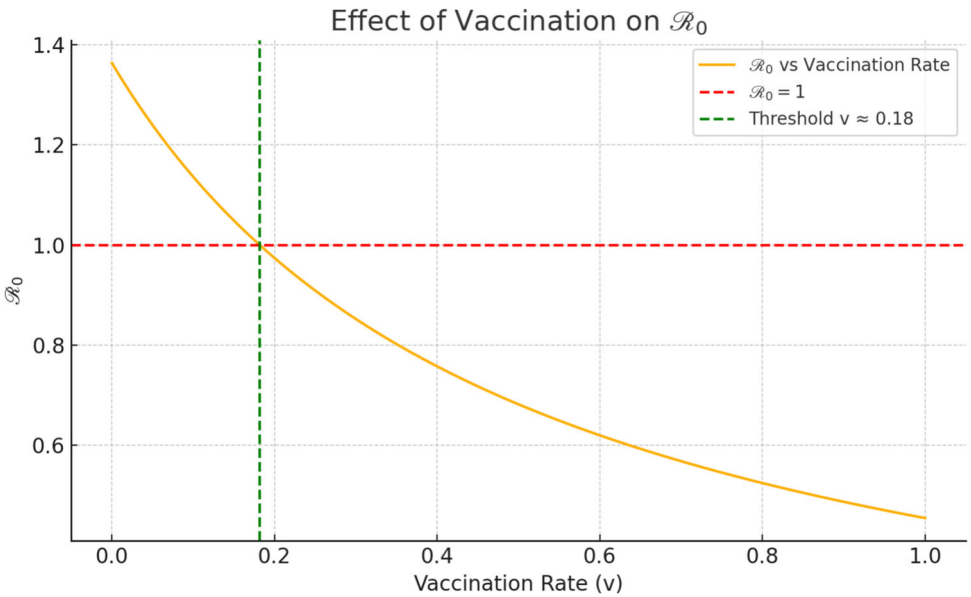


Fig. 3 Effect of increasing vaccination rate v on the basic reproduction number $\mathscr{R}_0$. The red dashed line indicates the threshold $\mathscr{R}_0 = 1$, and the green vertical line shows the critical vaccination rate ($v \approx 0.18$) beyond which transmission is no longer sustained

In our analysis of the local stability of the steady states, we employed standard linearization techniques. The key assumption underlying this analysis is that the system behaves locally like its Jacobian matrix evaluated at the equilibrium point. Specifically, we assume that the system is smooth and differentiable and that the dynamics near the equilibrium can be accurately captured by the linearized system.

To demonstrate the global stability of the disease-free equilibrium (DFE), we employed *Lyapunov's second method* in conjunction with *LaSalle's invariance principle*, both of which are standard tools in nonlinear dynamical systems theory. Lyapunov's second method involves constructing a suitable scalar function $V(t)$, known as a Lyapunov function, which is continuously differentiable, positive definite, and has a negative semi-definite time derivative along the trajectories of the system. In our analysis, we carefully constructed such a Lyapunov function to reflect the dynamics of the exposed and infectious compartments, ensuring that $V(t) = 0$ only at the DFE. While Lyapunov's method can establish stability, it typically guarantees only local or asymptotic stability unless the derivative $\dot{V}(t)$ is negative definite. This is where *LaSalle's invariance principle* becomes crucial. LaSalle's principle extends Lyapunov's method by allowing $\dot{V}(t)$ to be negative semi-definite and then identifying the largest invariant set within the region where $\dot{V}(t) = 0$. If the only solution that remains in this set is the equilibrium itself, then global asymptotic stability can be concluded.

7.1 Local Stability of $\mathscr{E}_0$

Theorem 4 *If $\mathscr{R}_0 < 1$, the disease-free equilibrium $\mathscr{E}_0$ given by (18) is locally asymptotically stable, and unstable if $\mathscr{R}_0 > 1$.*

Proof This result is an application of Theorem 2 in [60]. For the disease-free equilibrium (DFE), the local stability condition is based on the basic reproduction number $\mathscr{R}_0$. If $\mathscr{R}_0 < 1$, all eigenvalues of the Jacobian matrix have negative real parts, implying that the DFE is locally asymptotically stable. In contrast, if $\mathscr{R}_0 > 1$, at least one eigenvalue has a positive real part, and the DFE becomes unstable. □

7.2 Local Stability of $\mathscr{E}_1$

Theorem 5 *If $\mathscr{R}_0 > 1$, the disease-present equilibrium $\mathscr{E}_1$ given by (21) is locally asymptotically stable, and unstable if $\mathscr{R}_0 < 1$.*

Proof The Jacobian of the system (1) at the endemic equilibrium $\mathscr{E}_1$ is as follows:

$$J(\mathscr{E}_1) = \begin{bmatrix} -d & p & 0 & 0 & 0 & 0 \\ 0 & -(d+p+v)\mathscr{R}_0 & 0 & -\beta S_1 & 0 & 0 \\ 0 & \beta I_1 & -(d+\sigma) & \beta S_1 & 0 & 0 \\ 0 & 0 & \sigma & -(d+\gamma) & 0 & 0 \\ 0 & 0 & 0 & \gamma & -d & 0 \\ 0 & v & 0 & 0 & 0 & -d \end{bmatrix}.$$

Hence, the characteristic polynomial of $J(\mathscr{E}_1)$ is as follows:

$$\begin{aligned} p(\lambda) &= (\lambda+d)^3 \begin{vmatrix} \lambda + (d+p+v)\mathscr{R}_0 & 0 & \beta S_1 \\ -\beta I_1 & \lambda + (d+\sigma) & -\beta S_1 \\ 0 & -\sigma & \lambda + (d+\gamma) \end{vmatrix}, \\ &= (\lambda+d)^3(\lambda^3 + c_2\lambda^2 + c_1\lambda + c_0). \end{aligned}$$

Here,

$$c_0 = a_1a_2a_3(\mathscr{R}_0 - 1), \qquad c_1 = a_1(a_2+a_3)\mathscr{R}_0,$$
$$c_2 = a_1\mathscr{R}_0 + a_2 + a_3,$$

where

$$a_1 = d + p + v$$
$$a_2 = d + \sigma$$
$$a_3 = d + \gamma.$$

The roots of $p(\lambda)$ are $-d$(with multiplicity 3), and the roots of $q(\lambda)$, where

$$q(\lambda) = \lambda^3 + c_2\lambda^2 + c_1\lambda + c_0.$$

The system (1) will be locally asymptotically stable at $\mathscr{E}_1$ if and only if all the roots of $p(\lambda)$ have negative real parts, which will be true if and only if all the roots of $q(\lambda)$ have negative real parts. By Routh-Hurwitz crieria [63–65], all the roots of q will have negative real parts iff $c_0 > 0, c_1 > 0, c_2 > 0$, and $c_1c_2 > c_0$. Since $a_1, a_2, a_3$are all positive, and$\mathscr{R}_0 > 0$, $c_1$andc_2, both are positive. Moreover, $c_1c_2 > c_0$ always as

$$\begin{aligned} c_1c_2 &= a_1(a_2+a_3)(a_1\mathscr{R}_0 + a_2 + a_3)\mathscr{R}_0 > a_1(a_2+a_3)^2\mathscr{R}_0 \\ &> 2a_1a_2a_3\mathscr{R}_0 > a_1a_2a_3(\mathscr{R}_0 - 1) = c_0. \end{aligned}$$

Finally, $c_0 = a_1a_2a_3(\mathscr{R}_0 - 1)$ will be positive if and only if $\mathscr{R}_0 > 1$. Thus, the theorem. □

Our findings are consistent with the classical results in epidemic modeling. Local stability results are inherently limited

to small perturbations around the equilibrium. Structural changes to the model, such as adding delays, age structure, or stochastic effects, could alter the system's dynamics and potentially affect stability outcomes. However, while the numerical value of $\mathscr{R}_0$ is sensitive to key parameters such as β, σ and γ, the qualitative criterion of stability ($\mathscr{R}_0 < 1$) remains a robust and reliable indicator for any variation in parameters.

7.3 Global Stability of $\mathscr{E}_0$

Together, Lyapunov's second method and LaSalle's invariance principle provide a powerful and complementary framework for establishing global stability, even in complex compartmental models like PSLIRV. In our study, we applied the LaSalle invariance principle to show that, under the condition ($\mathscr{R}_0 < 1$), the disease-free equilibrium attracts all trajectories in the feasible region. This combination of methods allowed us to rigorously prove the global stability of the DFE without requiring exact solutions to the nonlinear system. We have the following theorem.

Theorem 6 *The disease-free equilibrium $\mathscr{E}_0$ is globally asymptotically stable on Δ if $\mathscr{R}_0 \leq 1$.*

Proof Consider the following Lyapunov function:

$$\mathbf{E}(Y(t)) = u^T W^{-1} y(t), \tag{24}$$

where $Y(t) = (P(t), V(t), S(t), L(t), I(t), R(t))$ is the state vector, $y(t) = (L(t), I(t))$ is the infected state vector, and $u = [0 \;\; 1]^T$ is a left eigen vector of $W^{-1}F$ w.r.t. $\mathscr{R}_0$, with F & W as obtained in Sect. 4.2. Note that $\mathbf{E}$ is a well-defined function since there is a one-to-one correspondence between $Y(t) \longleftrightarrow y(t)$. Now, $\mathbf{E}$ satisfies the following:

$$\begin{cases} \mathbf{E}(\mathscr{E}_0) = 0, \\ \mathbf{E}(Y(t)) > 0 \text{ if } Y(t) \neq \mathscr{E}_0, \text{ and,} \\ \mathbf{E}(Y(t)) \text{ is unbounded radially: } \|Y\| \to \infty \implies \mathbf{E}(Y(t)) \to \infty. \end{cases} \tag{25}$$

Now, by evaluating $\mathbf{E}$'s time derivative along model (1)'s trajectory in the Δ region, we obtain

$$\begin{aligned} \frac{d\mathbf{E}}{dt} &= u^T W^{-1} \dot{y} \\ &\leq u^T W^{-1}(F - W)y \\ &\leq (u^T W^{-1} F - u^T W^{-1} W)y \\ &\leq (u^T \mathscr{R}_0 - u^T)y \\ &\leq (\mathscr{R}_0 - 1)u^T y \end{aligned}$$

Therefore, if $\mathscr{R}_0 \leq 1$, $\frac{d\mathbf{E}(Y)}{dt} \leq 0$. Further, $\frac{d\mathbf{E}(Y)}{dt} = 0$ iff y is the zero vector, which happens exactly when the system is at the disease-free equilibrium $\mathscr{E}_0$ amongst the feasible solutions, i.e., $Y = \mathscr{E}_0$. This means that the set

$$\mathbf{E}_{\mathscr{E}_0} = \left\{ Y \in \Delta : \dot{\mathbf{E}} = 0 \right\} = \{\mathscr{E}_0\}, \tag{26}$$

is the singleton $\mathscr{E}_0$. Following Lasalle's invariance principle [66–69], therefore, $\mathscr{E}_0$ is globally asymptotically stable in Δ if $\mathscr{R}_0 \leq 1$. □

8 The Optimal Control Problem

This section employs the concept of optimal control, a rigorous approach to studying infectious disease dynamics. By implementing the most efficient intervention strategies, the objective is to minimize the number of infected individuals while ensuring that the associated costs remain as low as feasible. We perform a theoretical analysis along with numerical simulations to illustrate the impact of these control measures on the spread of the COVID-19 virus.

In the optimal control formulation, we considered two primary control strategies:

- **Self-protection efforts** ($u_1(t)$): This control represents non-pharmaceutical interventions such as wearing masks, social distancing, and hand hygiene. It reduces the effective contact rate and shifts individuals from the susceptible to the self-protected class.
- **Vaccination** ($u_2(t)$): This control models the administration of vaccines to susceptible individuals, moving them into the vaccinated class, thereby directly reducing the susceptible pool and interrupting transmission chains.

These controls are incorporated into the model as time-dependent functions and are bounded between 0 and 1, reflecting resource limitations and practical feasibility. The interaction among these strategies is both synergistic and complementary. For example:

- Increasing self-protection reduces new infections, thereby lowering the burden on vaccination.
- Vaccination directly reduces the susceptible population and indirectly supports the effectiveness of self-protection by decreasing exposure risk.

In the objective functional, each control is associated with a quadratic cost term, capturing the economic or logistical burden of implementing the strategy. The optimal control solution seeks to balance infection reduction with total intervention cost. The results show that a coordinated

strategy—where both controls are applied dynamically over time—achieves a greater reduction in infections and total cost than any single intervention alone. The model thus highlights the importance of integrated, time-sensitive public health responses.

In our model (1), we allow the self-protection rate and vaccination rate to be a function of time $u_1(t)$ and $u_2(t)$, respectively, treating them as control variables. Thus, $u_1(t)$ represents the proportion of the susceptible population becoming protected at time t, whereas $u_2(t)$ represents the fraction of susceptible individuals vaccinated at time t. With this interpretation, model (1) with two controls takes this form:

$$\begin{cases} \frac{dP(t)}{dt} = u_1(t)S - dP, \\ \frac{dS(t)}{dt} = b - \beta IS - (d + u_1(t) + u_2(t))S, \\ \frac{dL(t)}{dt} = \beta IS - (d+\sigma)L, \\ \frac{dI(t)}{dt} = \sigma L - (d+\gamma)I, \\ \frac{dR(t)}{dt} = \gamma I - dR, \\ \frac{dV(t)}{dt} = u_2(t)S - dV, \end{cases} \tag{27}$$

with initial conditions as stated in (2).

We want to simultaneously minimize the number of population in the latent phase of infection, and infectious individuals, the cost of self-protection, and the expense of vaccination. Hence, we define the objective functional as follows:

$$J\left(u_1(t), u_2(t)\right) = \int_0^T \left[\varphi_1 L + \varphi_2 I + \frac{1}{2}m_1 u_1^2 + \frac{1}{2}m_2 u_2^2\right] dt, \tag{28}$$

with $\varphi_1, \varphi_2, m_1, m_2$ being positive weight constants that serve to balance the units of the integrand, and representing the relative costs of each associated term over the interval $[0, T]$. The admissible set of controls $u(t) = (u_1(t), u_2(t))$ is defined as follows:

$$U = \{u : [0, \infty) \to [0, 1] \times [0, 1] \text{ such that } u \text{ is measurable}, t \in [0, T]\}. \tag{29}$$

We hence look for an optimal control u^* in U so that

$$J(u^*) = \min\{J(u) : u \in U\}.$$

8.1 Existence of Optimal Control

We now investigate the existence of an optimal control pair for (27), (28). Using the results of [70], we shall demonstrate the existence of an optimal control pair.

Theorem 7 *A control pair $u^* = (u_1^*, u_2^*) \in U$, minimizing the objective functional $J(u_1(t), u_2(t))$ for the control system (27) and (28) exists.*

Proof We let $\mathcal{L}$ denote the integrand of J, i.e., $\mathcal{L} := \varphi_1 L + \varphi_2 I + \frac{1}{2}m_1 u_1^2 + \frac{1}{2}m_2 u_2^2$. Note that the system (27)'s solutions are bounded for any finite time interval. To apply Corollary 4.1 in [70], we verify the following five conditions:

1. $\mathcal{L}$ is convex on U.
2. U is closed as well as convex.
3. Linear functions in state variables bind the state system.
4. The set of controls and respective state variables are non-empty.
5. There are positive constants m, k, and $n > 1$ that satisfies the following: $\mathcal{L} + m \geq k\left(u_1^2 + u_2^2\right)^{\frac{n}{2}}$.

First, clearly, $\mathcal{L}$ is convex on u. Secondly, U is closed as well as convex by definition. Since state solutions of model (27) are bounded, the third condition is satisfied too. As the system (27) has bounded coefficients, the fourth condition follows from Carathéodory's theorem [71]. Lastly, because $\varphi_1, \varphi_2, m_1, m_2, L, I$ are all positive, and u_1 & u_2 both are bounded between 0 & 1, we have the following:

$$\mathcal{L} + m \geq \frac{1}{2}m(u_1^2 + u_2^2 + 2) \geq \frac{m}{2}(u_1^2 + u_2^2)^2,$$

where $m = \min\{m_1, m_2\} > 0$, and thereby giving the last requisite property. By Theorem 4.1 of [70], we conclude that there exists an optimal control pair $\left(u_1^*, u_2^*\right)$ such that

$$J\left(u_1^*, u_2^*\right) = \min\{J(u_1, u_2) : (u_1, u_2) \in U\}.$$

Thus, $u^*(t) = (u_1^*(t), u_2^*(t))$ is a pair of optimal control in U as claimed. □

8.2 Characterization of Optimal Control

We apply Pontryagin's maximum principle [71–73] to obtain the necessary conditions for the optimal control problem (27), (28).

Theorem 8 *For the optimal control $u^*(t)$ with solutions $X^* = (P^*, S^*, L^*, I^*, R^*, V^*)$ of (27) minimizing the objective functional (28), there are costate variables $\lambda_P, \lambda_S, \lambda_L, \lambda_I, \lambda_R$, and λ_V that satisfies the following adjoint equations:*

$$\begin{aligned}
\dot{\lambda_P} &= \lambda_P d,\\
\dot{\lambda_S} &= \lambda_S(d+u_1^*+u_2^*)+(\lambda_S-\lambda_L)\beta I^*-(\lambda_P u_1^*+\lambda_V u_2^*),\\
\dot{\lambda_L} &= -\left[\varphi_1+(\lambda_I-\lambda_L)\,\sigma-\lambda_L d\right],\\
\dot{\lambda_I} &= -\left[\varphi_2+(\lambda_L-\lambda_S)\,\beta S^*+(\lambda_R-\lambda_I)\gamma-\lambda_I d\right],\\
\dot{\lambda_R} &= \lambda_R d,\\
\dot{\lambda_V} &= \lambda_V d,
\end{aligned}$$

with conditions of transversality that the costate variables vanish at $t = T$.

In addition, the optimal control pair $u^*(t) = (u_1^*(t), u_2^*(t))$ is

$$\begin{aligned}
u_1^* &= \max\left\{0, \min\left\{\frac{(\lambda_S-\lambda_P)\,S^*}{m_1}, 1\right\}\right\},\\
u_2^* &= \max\left\{0, \min\left\{\frac{(\lambda_S-\lambda_V)\,S^*}{m_2}, 1\right\}\right\}.
\end{aligned}$$

Proof The maximum principle [71–73] of Pontryagin is applied to our system (27) and (28). In order to do so, for $t \in [0, T]$, Hamiltonian H is defined as follows:

$$\begin{aligned}
H &= \varphi_1 L+\varphi_2 I+\frac{1}{2}m_1u_1^2+\frac{1}{2}m_2u_2^2+\lambda_P\dot{P}+\lambda_S\dot{S}\\
&\quad+\lambda_L\dot{L}+\lambda_I\dot{I}+\lambda_R\dot{R}+\lambda_V\dot{V}\\
&= \varphi_1 L+\varphi_2 I+\frac{1}{2}m_1u_1^2+\frac{1}{2}m_2u_2^2+\lambda_P\left[u_1S-dP\right]\\
&\quad+\lambda_S\left[b-\beta IS-(d+u_1+u_2)S\right]\\
&\quad+\lambda_L\left[\beta IS-(d+\sigma)L\right]+\lambda_I\left[\sigma L-(d+\gamma)I\right]\\
&\quad+\lambda_R\left[\gamma I-dR\right]+\lambda_V\left[u_2S-dV\right],
\end{aligned}$$

where $\lambda_P, \lambda_S, \lambda_E, \lambda_I, \lambda_R$, and λ_V are the adjoint or costate variables. As a consequence of Pontryagin's maximum principle, the following equalities are satisfied by the adjoint variables:

$$\begin{aligned}
\dot{\lambda_P} &= -\frac{\partial H}{\partial P}, \quad \dot{\lambda_S} = -\frac{\partial H}{\partial S}, \quad \dot{\lambda_L} = -\frac{\partial H}{\partial L},\\
\dot{\lambda_I} &= -\frac{\partial H}{\partial I} \quad \dot{\lambda_R} = -\frac{\partial H}{\partial R}, \quad \dot{\lambda_V} = -\frac{\partial H}{\partial V},
\end{aligned}$$

with the transversality conditions: $\lambda_P(T) = \lambda_S(T) = \lambda_L(T) = \lambda_I(T) = \lambda_R(T) = \lambda_V(T) = 0$. Now, optimality condition at $u(t) = u^*(t)$ gives:

$$\left.\frac{\partial H}{\partial u_1}\right|_{u_1(t)=u_1^*(t)} = \left.\frac{\partial H}{\partial u_2}\right|_{u_2(t)=u_2^*(t)} = 0,$$

i.e.,

$$\begin{aligned}
m_1u_1+S^*(\lambda_P-\lambda_S) &= m_2u_2+S^*(\lambda_V-\lambda_S)\\
&= 0 \text{ at } u = u^*.
\end{aligned} \tag{30}$$

On solving (30) for $u^* = (u_1^*, u_2^*)$, we get

$$\begin{cases}
u_1^*(t) = \dfrac{(\lambda_S-\lambda_P)\,S^*}{m_1}, \text{ and}\\
u_2^*(t) = \dfrac{(\lambda_S-\lambda_V)\,S^*}{m_2} \quad \text{on condition that } u^*(t) \in U.
\end{cases} \tag{31}$$

Then, (31) along with bounds for "$u^* \in U$" from (29) characterizes the optimal control as below:

$$u_1^*(t) = \begin{cases}
0, & \text{if } \frac{(\lambda_S-\lambda_P)S^*}{m_1} \le 0,\\
\frac{(\lambda_S-\lambda_P)S^*}{m_1}, & \text{if } 0 \le \frac{(\lambda_S-\lambda_P)S^*}{m_1} \le 1,\\
1, & \text{if } \frac{(\lambda_S-\lambda_P)S^*}{m_1} \ge 1.
\end{cases}$$

and,

$$u_2^*(t) = \begin{cases}
0, & \text{if } \frac{(\lambda_S-\lambda_V)S^*(t)}{m_2} \le 0,\\
\frac{(\lambda_S-\lambda_V)S^*}{m_2}, & \text{if } 0 \le \frac{(\lambda_S-\lambda_V)S^*}{m_2} \le 1,\\
1, & \text{if } \frac{(\lambda_3-\lambda_4)I^*}{2B_2} \ge 1.
\end{cases}$$

That is, in short, as follows:

$$\begin{cases}
u_1^* = \max\left\{0, \min\left\{\dfrac{(\lambda_S-\lambda_P)\,S^*}{m_1}, 1\right\}\right\},\\
u_2^* = \max\left\{0, \min\left\{\dfrac{(\lambda_S-\lambda_V)\,S^*}{m_2}, 1\right\}\right\}.
\end{cases} \tag{32}$$

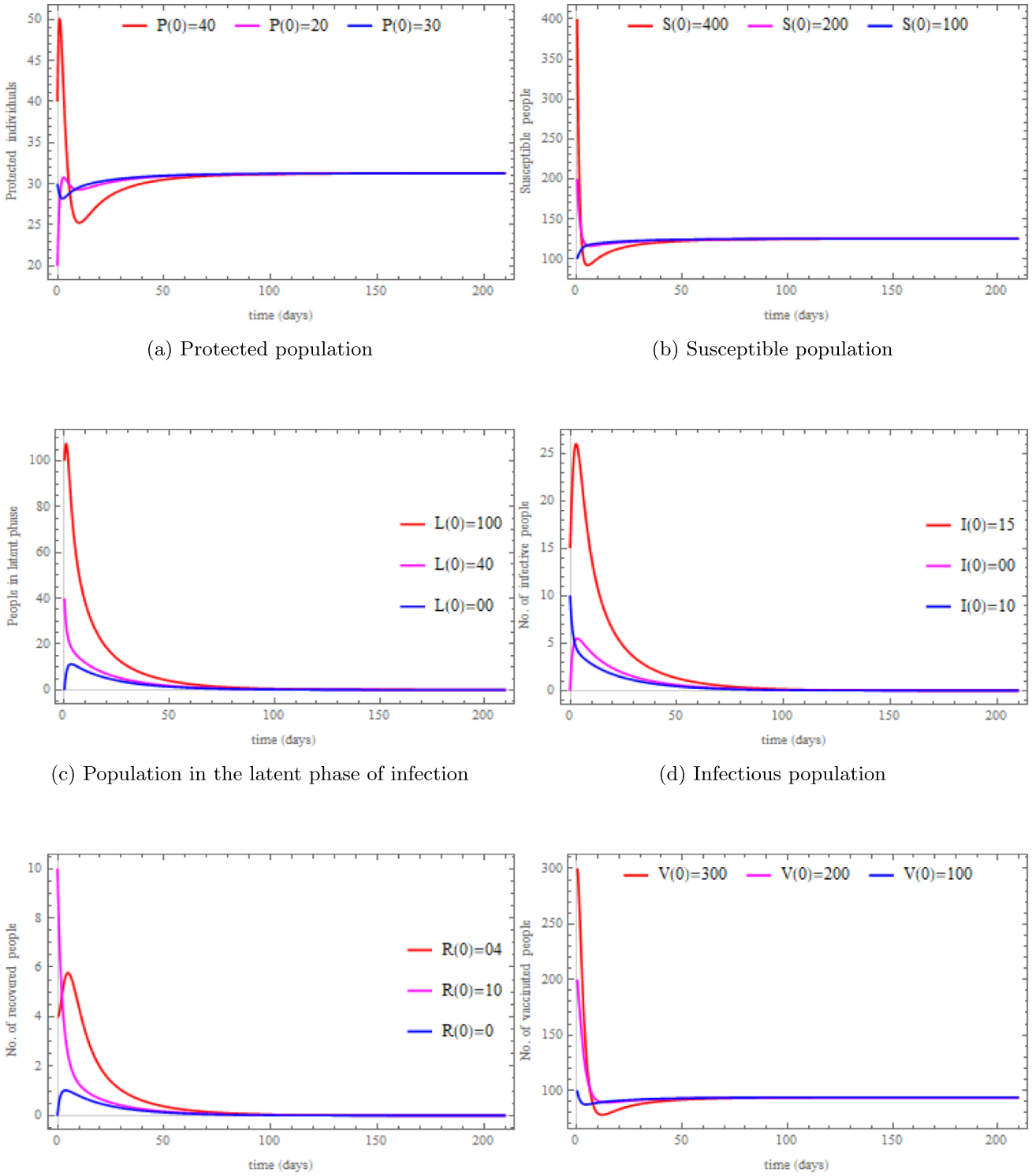
u^* in fact minimizes the Hamiltonian H as at $u = u^*$,

$$\frac{\partial^2 H}{\partial u_1^2} = m_1 > 0, \frac{\partial^2 H}{\partial u_2^2} = m_2 > 0, \text{ and}$$

$$\frac{\partial^2 H}{\partial u_1^2}\frac{\partial^2 H}{\partial u_2^2}-\left(\frac{\partial^2 H}{\partial u_1 \partial u_2}\right)^2 = m_1m_2 > 0.$$

Table 1 Parameter values for Fig. 4

Parameter	Values
b	100
β	0.0125
γ	0.1
d	0.4
σ	0.15
p	0.1
v	0.3



(a) Protected population

(b) Susceptible population

(c) Population in the latent phase of infection

(d) Infectious population

(e) Recovered population

(f) Vaccinated population

Fig. 4 The system (1) asymptotically approaches $\mathscr{E}_0 = (31, 125, 0, 0, 0, 94)$ for $\mathscr{R}_0 = 0.852 < 1$

Table 2 Parameter values for Fig. 5

Parameter	Values
b	100
β	0.0125
γ	0.1
d	0.4
σ	0.15
p	0.1
v	0.1

Using (32), we obtain the optimality system $X^* = (P^*, , V^*, S^*, L^*, I^*, R^*)$ for (27) that corresponds to the optimal control $u^* = (u_1^*, u_2^*)$ as follows:

$$\begin{cases} \frac{dP^*}{dt} = u_1^* S^* - dP^*, \\ \frac{dS^*}{dt} = b - \beta I^* S^* - (d + u_1^* + u_2^*)S^*, \\ \frac{dL^*}{dt} = \beta I^* S^* - (d + \sigma)L^*, \\ \frac{dI^*}{dt} = \sigma L^* - (d + \gamma)I^*, \\ \frac{dR^*}{dt} = \gamma I^* - dR^*, \\ \frac{dV^*}{dt} = u_2^* S^* - dV^*, \end{cases} \tag{33}$$

with initial conditions: $P^*(0) \geq 0, S^*(0) \geq 0, L^*(0) \geq 0, I^*(0) \geq 0, R^*(0) \geq 0, V^*(0) \geq 0$, and the corresponding adjoint variables satisfies

$$\begin{aligned} \dot{\lambda_P} &= \lambda_P d, \\ \dot{\lambda_S} &= \lambda_S(d + u_1^* + u_2^*) + (\lambda_S - \lambda_L)\beta I^* - (\lambda_P u_1^* + \lambda_V u_2^*), \\ \dot{\lambda_L} &= -[\varphi_1 + (\lambda_I - \lambda_L)\sigma - \lambda_L d], \\ \dot{\lambda_I} &= -\left[\varphi_2 + (\lambda_L - \lambda_S)\beta S^* + (\lambda_R - \lambda_I)\gamma - \lambda_I d\right], \\ \dot{\lambda_R} &= \lambda_R d, \\ \dot{\lambda_V} &= \lambda_V d, \end{aligned}$$

with the transversality conditions: $\lambda_P(T) = \lambda_S(T) = \lambda_L(T) = \lambda_I(T) = \lambda_R(T) = \lambda_V(T) = 0$. The proof is now complete. □

Solving the optimal control problem provided several valuable insights into both the effectiveness and feasibility of implementing intervention strategies in real-world scenarios.

First, the model demonstrates that time-dependent, coordinated interventions—specifically self-protection and vaccination—are significantly more effective than isolated or static strategies. Optimal control trajectories reveal that early and intensive application of self-protection and vaccination can substantially reduce peak infection levels and flatten the epidemic curve. This aligns with public health observations during outbreaks like COVID-19, where timely and layered interventions were critical in managing transmission.

Second, the optimal control profiles suggest that interventions can often be relaxed over time without sacrificing long-term disease control, especially after reaching key thresholds in vaccination coverage or reductions in the infectious population. This provides practical guidance for policymakers on when to scale back interventions to minimize social and economic disruption.

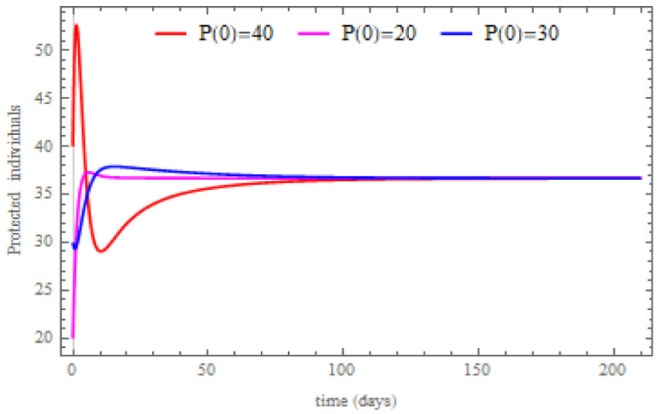
Third, by including control costs in the objective functional, the model captures trade-offs between epidemiological outcomes and resource constraints. This allows us to evaluate not just which strategies are effective, but also which are cost-effective. For instance, in scenarios with limited resources, the model may prioritize early self-protection and gradual vaccination over costly mass treatment campaigns.

Finally, the results underscore the importance of adaptive, data-informed policy: the optimal strategies depend sensitively on model parameters such as transmission and recovery rates, which can vary by region and over time. This highlights the need for real-time data integration and local calibration when applying such models in practice.

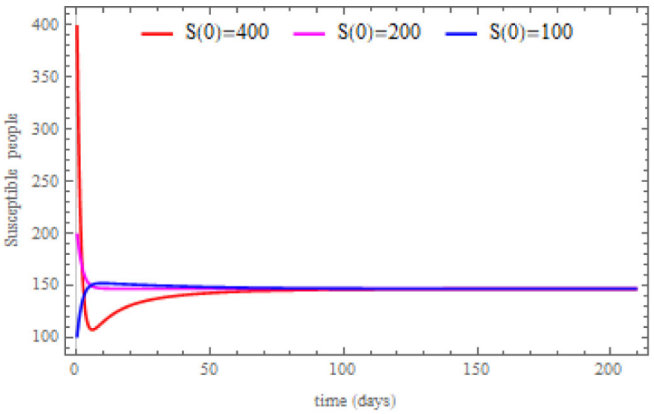
In summary, the optimal control framework offers actionable insights into how to time and coordinate interventions to achieve maximum impact with limited resources, supporting evidence-based public health planning.

9 Simulations

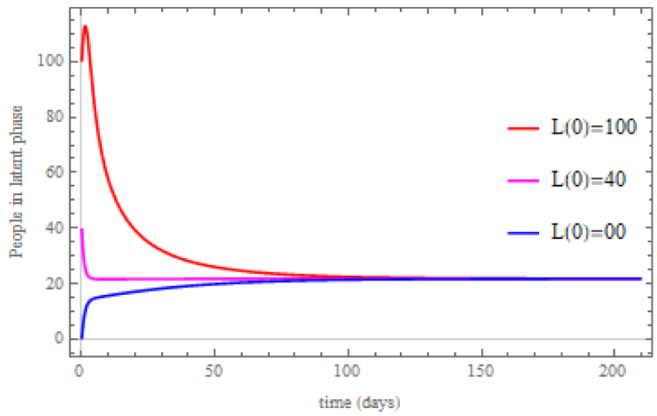
We performed extensive numerical simulations to validate our theoretical findings under various initial conditions and parameter scenarios. These simulations served two key purposes: (1) to verify the analytical results concerning stability and optimal control and (2) to explore the model's behavior beyond the limitations of linearized or local analysis. There are two parts to this section. The first part is devoted to verifying the analytical findings discussed in Sect. 3, 4, 5, 6, and 7. In the second part, we solve the optimal control problem of Sect. 8 numerically by applying the Pontryagin's maximum principle, resulting in a coupled system of state and adjoint differential equations. We employ the forward-backward sweep method combined with the fourth-order Runge–Kutta (RK4) integration scheme for both the state and adjoint systems. The RK4 method provides a good balance between accuracy and computational cost. Its higher-order accuracy allows us to use relatively larger time steps while maintaining numerical stability, which is essential for the iterative



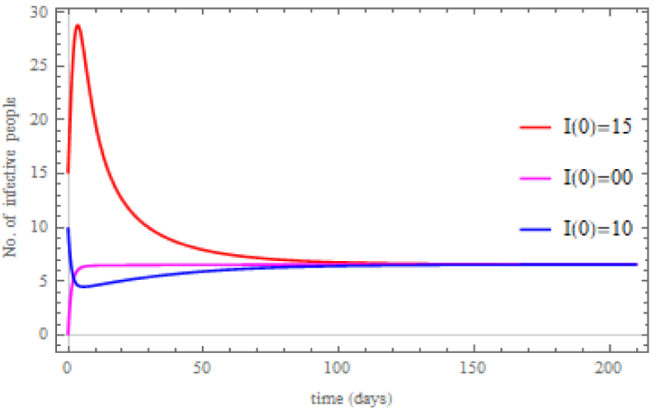
(a) Protected population



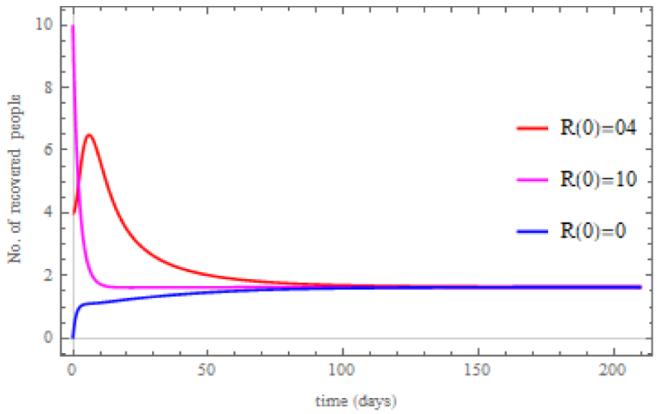
(b) Susceptible population



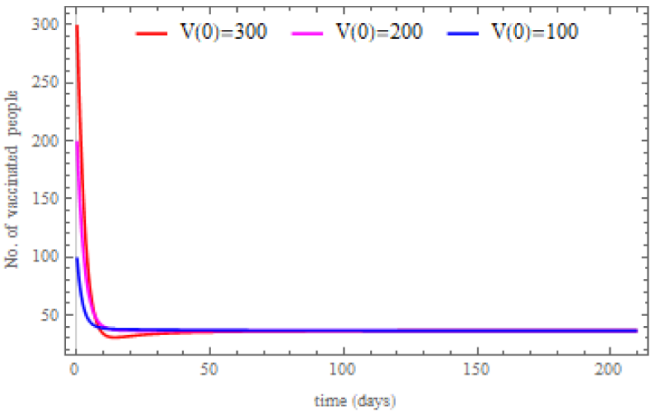
(c) Population in the latent phase of infection



(d) Infectious population



(e) Recovered population



(f) Vaccinated population

Fig. 5 The system (1) approaches $\mathscr{E}_1 = (37, 147, 22, 7, 2, 37)$ asymptotically for $\mathscr{R}_0 = 1.136 > 1$

nature of the forward-backward sweep. In our simulations, the method demonstrates fast convergence—typically within a few iterations—and remains computationally efficient for long time horizons. In terms of scalability, while the number of computations increases with the addition of more state variables or control components, the method still performs well for models like PSLIRV. For substantially more complex models (e.g., with age structure or spatial heterogeneity), advanced solvers or parallel computing may be necessary to maintain computational efficiency. To substantiate our findings, the initial values of the sub-population will be changed in the various compartments of model (1).

The initial conditions for each compartment were chosen based on a hypothetical outbreak scenario in a closed population. For example, a small proportion of the population was initially infected or exposed (e.g., $I(0) = 5$, $L(0) = 3$), while the majority were susceptible. The initial sizes of the self-protected and vaccinated compartments were set to reflect early-stage behavioral and public health response levels. Using the formula $N(0) = P(0) + S(0) + L(0) + I(0) + R(0) + V(0)$, the total initial population is calculated for each circumstance.

9.1 Without Controls

In order to demonstrate the dependence of stability on $\mathscr{R}_0$, we adopt two sets of parameter values corresponding respectively to $\mathscr{R}_0 \leq 1$ and $\mathscr{R}_0 > 1$. Also, we shall be using different vaccination rate v to highlight the effect of vaccination on disease eradication.

For the first set of numerical simulations, the parameter values specified in Table 1 are utilized. $\mathscr{R}_0$ is 0.852, and $\mathscr{E}_0 = (31, 125, 0, 0, 0, 94)$ in this case. The dynamics of the system (1) is presented in Fig. 4. It is seen from Fig. 4 that for any initial values of sub-population, P, S, and V approaches their respective disease-free steady state, whereas L, I, and R goes to zero. This shows that when $\mathscr{R}_0 < 1$, $\mathscr{E}_0$ is both locally and globally asymptotically stable, and thus in agreement with Theorems 4 and 6.

For the next set of simulations, parameter values from Table 2 are utilized. The BRN $\mathscr{R}_0$ is 1.136, and the disease-present equilibrium is $\mathscr{E}_1 = (37, 147, 22, 7, 2, 37)$ in this case. The dynamics of the system (1) is presented in Fig. 5. It is seen from Fig. 5 that for any initial sub-population, the state vector (P, S, L, I, R, V) approach the endemic equilibrium point $\mathscr{E}_1$. This shows that when $\mathscr{R}_0 > 1$, $\mathscr{E}_0$ is unstable but $\mathscr{E}_1$ is stable, and thus in agreement with Theorems 5 and 6.

The parameter values in Table 3 are utilized for the last case. We will use variable vaccination rate $v \in \{0\%, 10\%, 20\%, 60\%\}$. The dynamics of the system (1) is presented in Fig. 6. We note that when there is no vaccination, or $v = 10\%$, the BRN $\mathscr{R}_0$ is greater than 1; but for $v = 20\%$ or $v = 60\%$, $\mathscr{R}_0$ is less than 1. From Fig. 6, it is seen that in the first two scenarios, the state vector asymptotically approaches the respective endemic equilibrium $\mathscr{E}_1$, whereas, in the last two scenarios, the state vector asymptotically approaches the respective disease-free equilibrium $\mathscr{E}_0$. This again confirms Theorems 4, 5, and 6. Moreover, Fig. 6 shows that it is possible to eradicate the disease by sufficient vaccination, as observed in Sect. 6.

Table 3 Parameter values for Fig. 6

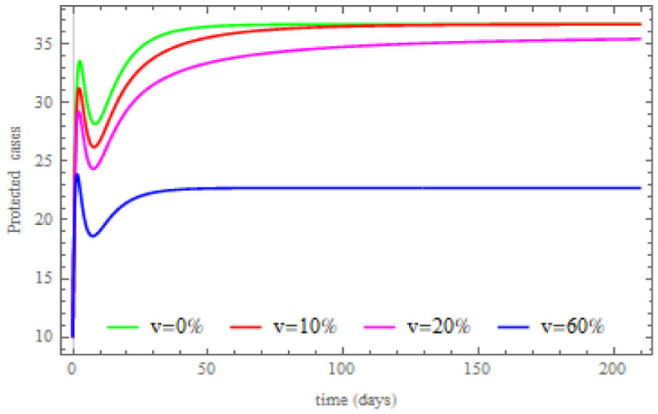
Parameter	Values
b	100
β	0.0125
γ	0.1
d	0.4
σ	0.15
p	0.1

9.2 With Controls

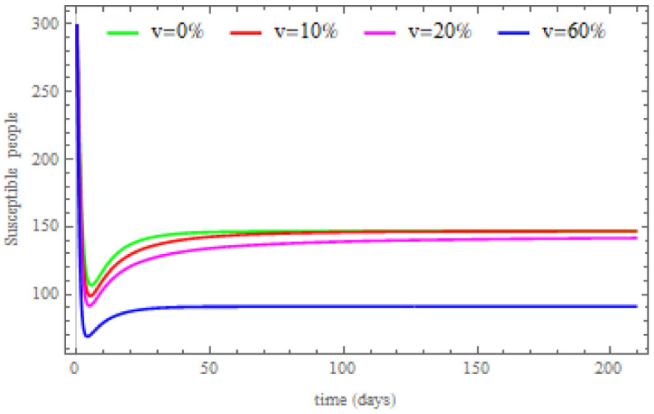
To formulate the optimal control problem, controls $u_1(t)$ & $u_2(t)$ were introduced, resulting in reduced susceptibility through self-protection and vaccination, respectively, and aimed at minimizing the costs associated with them as described in (28). We have conducted simulations to examine the outcomes of these optimal control mechanisms and compare them to uncontrolled situations. For the solution of the controlled system (27) and its adjoint system, parameter values listed in Table 4 are utilized. In this case, we have $\mathscr{R}_0 = 1.57895 > 1$.

In Fig. 7, we exhibit a comparative time series of the susceptible, exposed, and infective populations in all four cases: without any control($u_1 = 0, u_2 = 0$), with control self-protection alone ($u_2 = 0$), with only vaccination control ($u_1 = 0$), and with both of the optimal controls ($u_1 \neq 0, u_2 \neq 0$) for a period of 100 days. As illustrated in Fig. 7 a, b and c, the level of susceptible population S, the population in the latent phase of infection L and infectious cases I obtained using both controls (self-protection and vaccination control) are substantially lower than those obtained using only one control (self-protection or vaccination) or no control. The conclusion that may be drawn from this finding is that "intervention approaches that include both self-protection and vaccination controls generate comparatively superior results."

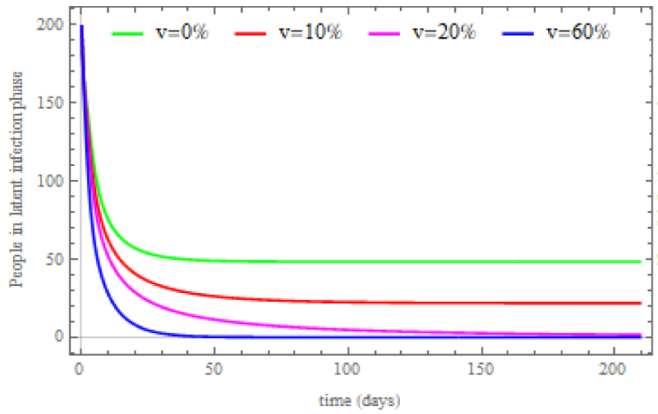
Finally, Fig. 8 shows the variation of optimal controls over 100 days. Figure 8a shows the control self-protection when



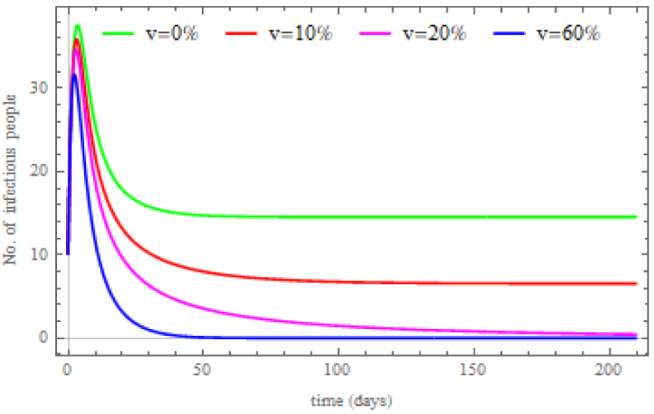
(a) Protected population



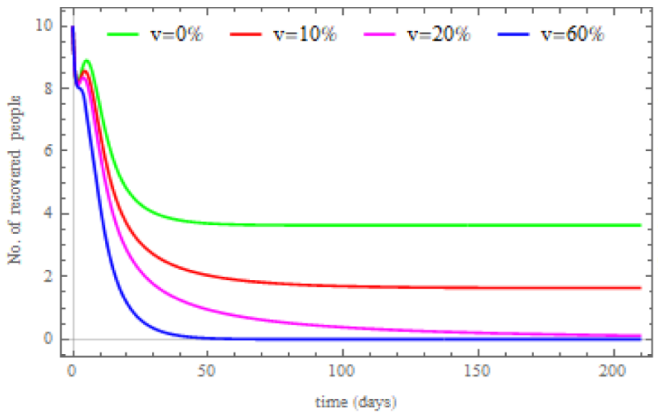
(b) Susceptible population



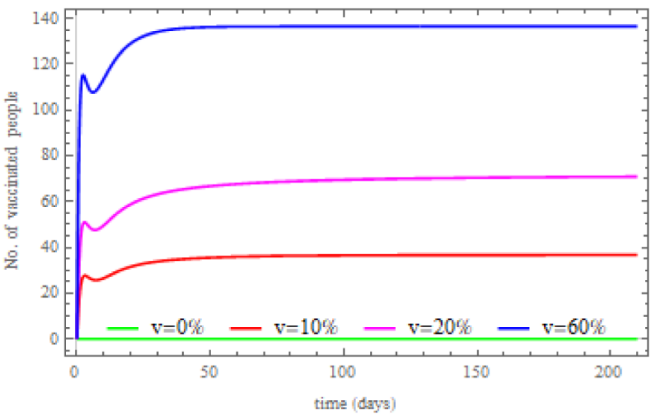
(c) population in the latent phase of infection



(d) Infectiouse population



(e) Recovered population



(f) Vaccinated population

Fig. 6 The system (1) under different vaccination scenario: $v \in \{0\%, 10\%, 20\%, 60\%\}$

Table 4 Parameter values for Figs. 7 and 8

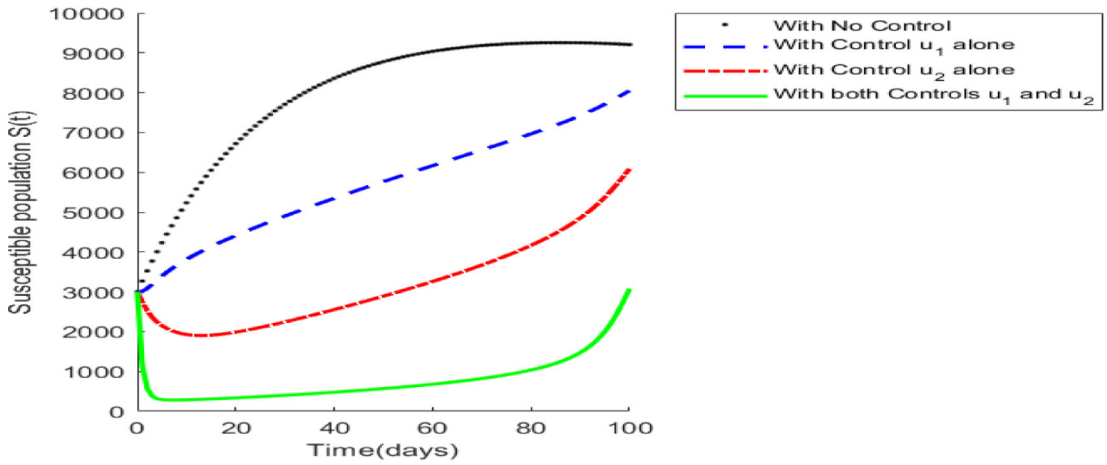
Parameter	Values
b	400
β	0.1
γ	0.01
d	0.04
σ	0.15
φ_1	1
φ_2	5
m_1	40
m_2	20

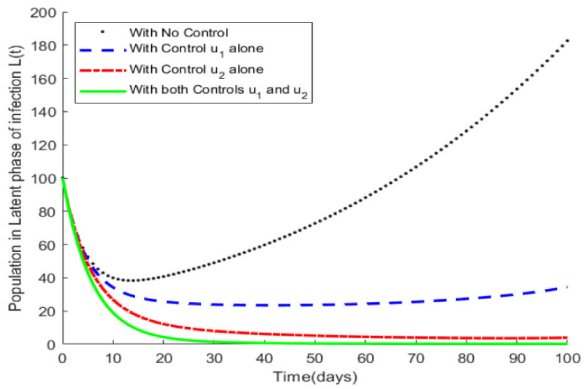
there is no vaccination, Fig. 8b shows the vaccination control when there is no self-protection, and Fig. 8c shows the optimal control function when both the controls are in place.

To assess the robustness and generalizability of our findings, we conducted multiple simulations under varying initial conditions and parameter settings. These variations included different levels of initial infections, susceptible populations, and parameter values related to transmission, recovery, vaccination, and self-protection. Figure 9 shows the effect of vaccination and transmission rate on $\mathscr{R}_0$, while Fig. 10 shows the effect of self-protection and recovery rate on $\mathscr{R}_0$.

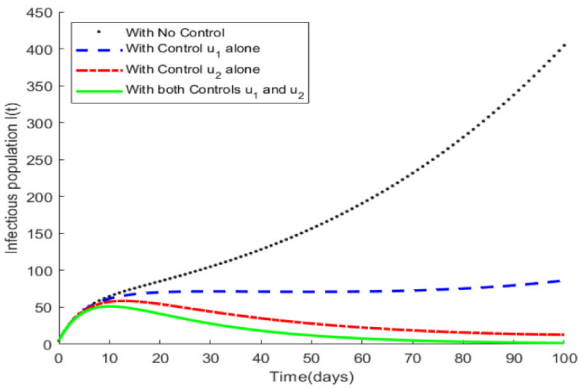
The results consistently demonstrated similar qualitative behavior: optimal intervention strategies—particularly early, well-timed application of self-protection effectively reduced the infection burden and total cost, regardless of the specific starting conditions. While the magnitude and duration of the epidemic varied across scenarios, the overall structure of the optimal control profiles remained robust, typically involving the following:

(a) Susceptible population



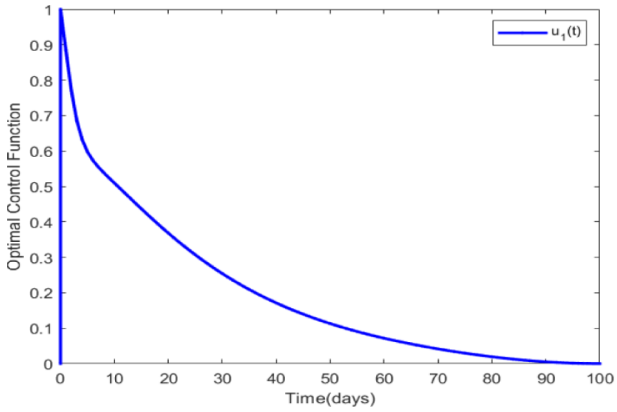


(b) Population in the latent phase of infection

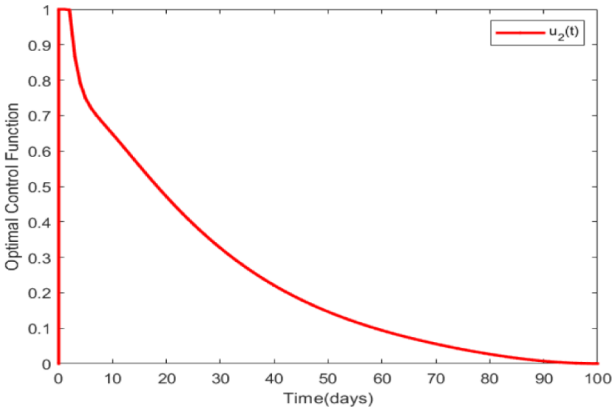


(c) Infective population

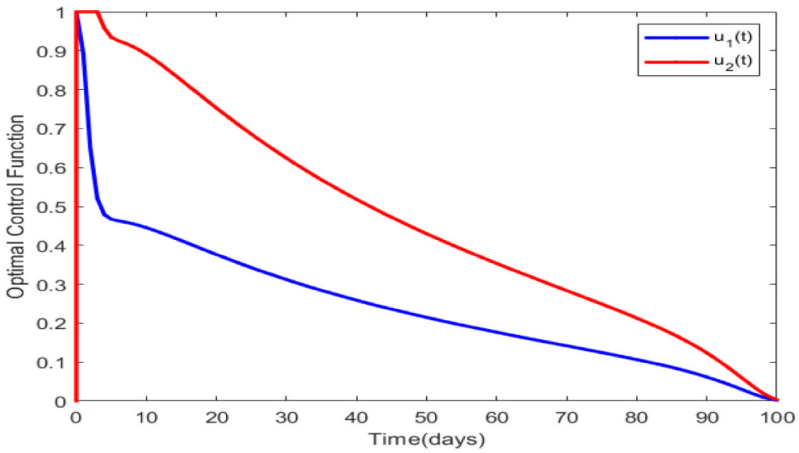
Fig. 7 Simulation of Model (1) with no control, with only one control, and with both controls for $\mathscr{R}_0 = 1.57895$. Better result is achieved when both controls are applied



(a) Control function u_1^* when $u_2(t) = 0$



(b) Control function u_2^* when $u_1(t) = 0$



(c) Optimal control function $u^* = (u_1^*, u_2^*)$ for self-protection and vaccination control when $u_1(t) \neq 0 \neq u_2(t)$

Fig. 8 Optimal control graphs

- High initial intensity of self-protection and vaccination to suppress transmission early
- A gradual reduction in control efforts as the epidemic came under control

These consistent patterns suggest that the model's insights are generalizable to a range of real-world settings and can be applied across different phases of an epidemic-whether early outbreak, peak, or decline, adjusting control intensities accordingly.

However, we acknowledge that the specific numerical outcomes (e.g., threshold vaccination rates or control costs) are sensitive to demographic and epidemiological parameters, which may vary between populations. Therefore, we recommend region-specific calibration when applying the model in practice. The current framework can accommodate such extensions and remains flexible for adaptation to different population structures, intervention capacities, or disease characteristics.

Overall, the simulations support the broader applicability of the model's conclusions, especially the importance of early, combined interventions and adaptive strategies in epidemic management.

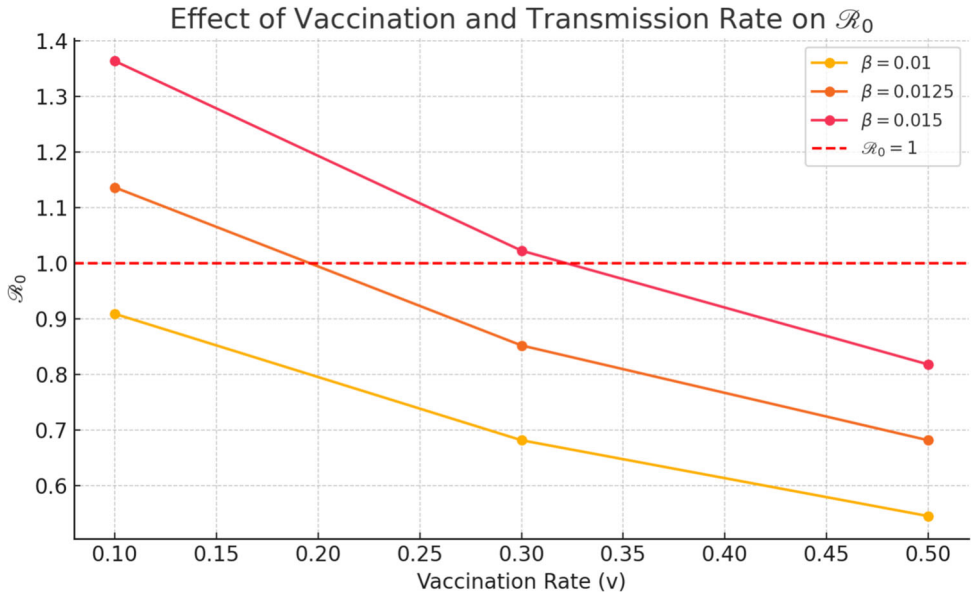


Fig. 9 Effect of varying vaccination rate v and transmission rate β on the basic reproduction number $\mathscr{R}_0$. Higher vaccination coverage significantly reduces $\mathscr{R}_0$ across all transmission scenarios. The red dashed line indicates the epidemic threshold at $\mathscr{R}_0 = 1$

10 Conclusion

This paper uses ordinary differential equations to develop a continuous-time mathematical model for the propagation of the COVID-19 virus. The basic properties of the model have been investigated, including positivity, boundedness, and invariant regions. The basic reproduction number is derived as $\mathscr{R}_0 = \frac{b\beta\sigma}{(d+\gamma)(d+\sigma)(d+p+v)}$. The relationship of $\mathscr{R}_0$ to the stability of the model has also been studied. We derived the equilibrium solutions of the model and established that the healthy equilibrium is LAS when $\mathscr{R}_0 < 1$, while the unhealthy equilibrium is LAS when $\mathscr{R}_0 > 1$. Moreover, for $\mathscr{R}_0 \leq 1$, the healthy equilibrium is GAS. Global stability has been established by considering the LaSalle invariance principle and an appropriate Lyapunov functional.

We have also demonstrated how vaccination affects COVID-19 dynamics. It has been shown that even though $\mathscr{R}_0$ can be more than 1 initially, enough vaccination can be brought below 1 so that the disease becomes extinct. Further, the higher the fraction of the vaccinated population, the less the spread of infection.

The final focus of this paper was on incorporating self-protection and vaccination as control strategies for susceptible individuals. Using these two controls, an appropriate problem of optimal control was developed for the model to minimize exposed and infected individuals, keeping cost in

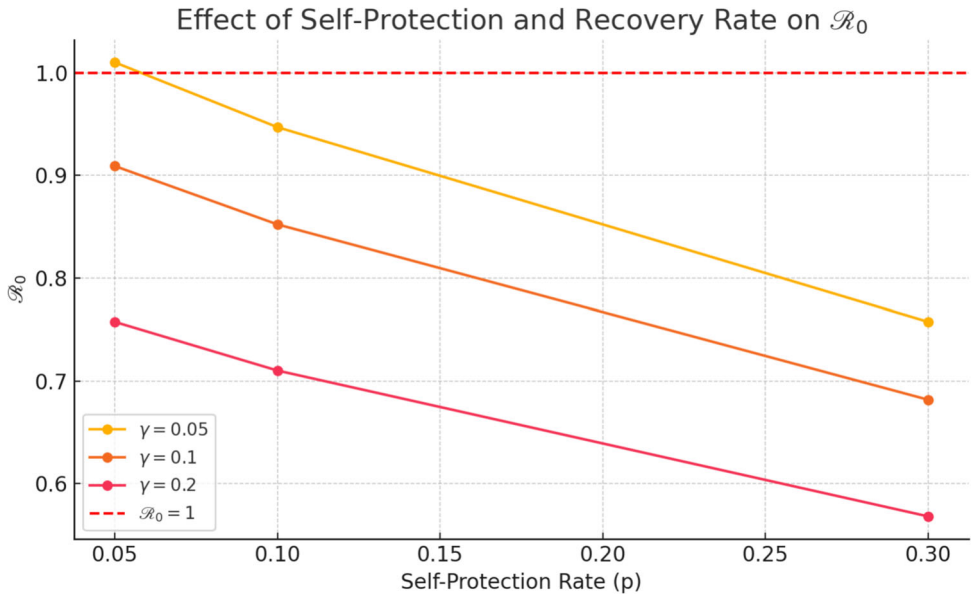


Fig. 10 Impact of self-protection rate p and recovery rate γ on the basic reproduction number $\mathscr{R}_0$. Increasing either parameter reduces $\mathscr{R}_0$, with stronger effects observed for higher recovery rates. The red dashed line indicates the epidemic threshold at $\mathscr{R}_0 = 1$

mind. We proved the existence of an optimal control pair, characterized it, and then solved it numerically. We found that the most effective way to decrease the prevalence of infections is to apply both controls simultaneously.

While the model captures the essential aspects of the transmission and control of disease, several simplifications must be taken into account. The assumption of homogeneous mixing does not reflect the heterogeneity of the population in the real world, and the model does not stratify by age, geography, or comorbidities. Parameter values are constant over time, and real-world complexities such as vaccine hesitancy, rollout delays, and reinfection are not explicitly modeled. Despite these limitations, the framework provides a strong theoretical basis for understanding the timing and interactions of the intervention. Although the model does not explicitly include variants, its flexible structure can be adapted for changing transmissibility or vaccine efficacy. This makes it a useful decision-support tool for preparing for variant-driven resurgences or new pathogens. Future work will focus on extending the model to include population heterogeneity, real-time parameter updates, spatial structure, and region-specific calibration using empirical data. These enhancements will improve the applicability of the model to inform localized public health strategies.

Author Contribution PBB: Original Draft, Writing, Conceptualization, Formal Analysis, Software. DR: Review, Reading and Editing, Formal Analysis. KD: Review, Investigation Supervision. BJN: Review, Validation, Supervision. HKS: Review, Visualization, Supervision.

Funding Open access funding provided by the Scientific and Technological Research Council of Türkiye (TÜBİTAK).

Data Availability No datasets were generated or analysed during the current study.

Declarations

Conflict of Interest The authors declare no competing interests.

Open Access This article is licensed under a Creative Commons Attribution 4.0 International License, which permits use, sharing, adaptation, distribution and reproduction in any medium or format, as long as you give appropriate credit to the original author(s) and the source, provide a link to the Creative Commons licence, and indicate if changes were made. The images or other third party material in this article are included in the article's Creative Commons licence, unless indicated otherwise in a credit line to the material. If material is not included in the article's Creative Commons licence and your intended use is not permitted by statutory regulation or exceeds the permitted use, you will need to obtain permission directly from the copyright holder. To view a copy of this licence, visit http://creativecommons.org/licenses/by/4.0/.

References

1. Centers for Disease Control and Prevention. 2020. Available online: https://www.cdc.gov/coronavirus/2019-nCoV/index.html
2. Johns Hopkins University and Medicine. 2020. Available online: https://coronavirus.jhu.edu
3. WHO official website https://www.who.int/emergencies/diseases/novel-coronavirus-2019/situation-reports/
4. A. Azmon, C. Faes, N. Hens, On the estimation of the reproduction number based on misreported epidemic data. Stat. Med. **33**, 1176–1192 (2014)
5. T. Burki, COVID-19 in Latin America. Lancet Infect. Dis. **20**, 547–548 (2020)
6. T.H.E. Alves, T.A. de Souza, S. Silva de Almeida, N.A. Ramos, S.V. de Oliveira, Underreporting of death by COVID-19 in Brazil's second most populous state. Front. Public Health **8**, (2020)
7. M. Saberi et al., Accounting for underreporting in mathematical modeling of transmission and control of COVID-19 in Iran. Front. Phys. **8**, 289 (2020)
8. M. Worobey, J.I. Levy et al., The Huanan market was the epicenter of SARS-CoV-2 emergence. Science (2022). https://doi.org/10.5281/zenodo.6299600
9. G. Gao et al., Surveillance of SARS-CoV-2 in the environment and animal samples of the Huanan Seafood Market, Preprint at Research Square (2022). https://doi.org/10.21203/rs.3.rs-1370392/v1
10. P. Zhou et al., A pneumonia outbreak associated with a new coronavirus of probable bat origin. NNature **579**, 270–273 (2020)
11. J. E. Pekar, A. Magee, E. Parker, N. Moshiri, K. Izhikevich, J. L. Havens, J. O. Wertheim et. al., SARS-CoV-2 emergence very likely resulted from at least two zoonotic events, Priprint, (2022), https://doi.org/10.5281/zenodo.6291628
12. A. Maxmen, Wuhan market was epicentre of pandemic's start, studies suggest. Nature **603**, 15–16 (2022)
13. Duduzile Ndwandwe, Charles S. Wiysonge, COVID-19 vaccines. Curr. Opin. Immunol. **71**, 111–116 (2021)
14. J. Johnson, Johnson & Johnson COVID-19 vaccine authorized by US FDA for emergency use-first single-shot vaccine in fight against global pandemic. (2021)
15. S.A. Levin, New directions in the mathematics of infectious disease, in *Mathematical Approaches for Emerging and Reemerging Infectious Diseases: Models, Methods, and Theory*. ed. by C. Castillo-Chavez, S. Blower, P. van den Driessche, D. Kirschner, A.-A. Yakubu (Springer, New York, New York, NY, 2002), pp.1–5
16. G. Chowell, C. Castillo-Chavez, P.W. Fenimore, C.M. Kribs-Zaleta, L. Arriola, J.M. Hyman, Model parameters and outbreak control for SARS. Emerg. Infect. Dis. **10**, 1258–1263 (2004)
17. K. Guedri, R. Zarin, A. Zeb et al., A numerical study of HIV/AIDS transmission dynamics and the onset of long-term disability in chronic infection. Eur. Phys. J. Plus **139** (2024). https://doi.org/10.1140/epjp/s13360-024-05881-x
18. R. Zarin, A. Khan, P. Kumar, U.W. Humphries, Fractional-order dynamics of Chagas-HIV epidemic model with different fractional operators. AIMS Mathematics **7**(10), 18897–18924 (2022). https://doi.org/10.3934/math.20221041
19. K. Guedri, R. Zarin, M. Oreijah, S.K. Alharbi, H.A.E. Khalifa, Modeling syphilis progression and disability risk with neural networks. Knowl.-Based Syst. **314** (2025). https://doi.org/10.1016/j.knosys.2025.113220
20. K. Guedri, R. Zarin, M. Oreijah, S.K. Alharbi, H.A.E. Khalifa, Artificial neural network-driven modeling of Ebola transmission dynamics with delays and disability outcomes. Comput. Biol. Chem. **115** (2025). https://doi.org/10.1016/j.compbiolchem.2025.108350

21. M.A. Ullah, N. Raza, M.Y. Alshahrani et al., Analysis and interpretation of a novel malaria transmission mathematical model with socioeconomic structure. Nonlinear Dyn. **113**, 12399–12418 (2025). https://doi.org/10.1007/s11071-024-10807-4
22. A. Omame, Q. Han, S.A. Iyaniwura, A. Ebenezer, N.L. Bragazzi, X. Wang, J.D. Kong, W.A. Woldegerima, Understanding the impact of HIV on mpox transmission in the MSM population: a mathematical modeling study. Infect. Dis. Modell. **9**(4), 1117–1137 (2024). https://doi.org/10.1016/j.idm.2024.05.008
23. A. Omame, S.A. Iyaniwura, Q. Han, A. Ebenezer, N.L. Bragazzi, X. Wang, W.A. Woldegerima, J.D. Kong, Dynamics of Mpox in an HIV endemic community: a mathematical modelling approach. Math. Biosci. Eng. **22**(2), 225–259 (2025). https://doi.org/10.3934/mbe.2025010
24. F. Brauer, C. Carlos, *Mathematical models in population biology and epidemiology*, vol. 2 (Springer, New York, 2012)
25. W.O. Kermack, A.G. McKendrick, A contribution to the mathematical theory of epidemics. Proc. R. Soc. Lond. A **115**(772), 700–721 (1927)
26. R.M. Anderson, B. Anderson, R.M. May, *Infectious diseases of humans: dynamics and control* (Oxford University Press, Oxford, 1992)
27. H.W. Hethcote, The mathematics of infectious diseases. SIAM Rev. **42**, 599–653 (2000)
28. R.M. May, R.M. Anderson, Population biology of infectious diseases: part II. Nature **280**(5722), 455–461 (1979)
29. M.S. Bartlett, *Stochastic population models in ecology and epidemiology* (Wiley, New York, 1960)
30. N.T.J. Bailey, *The mathematical theory of epidemics* (Griffin, London, 1957)
31. M.S. Bartlett, The critical community size for measles in the U. S. J. R. Stat. Soc. Ser. A **123**, 37–44 (1960)
32. M. Bartlett, Deterministic and stochastic models for recurrent epidemics, in *Proceedings of the Third Berkeley Symposium on Mathematical Statistics and Probability* vol. 4 (1956), pp. 109
33. Y. Hao et al., Prediction and analysis of corona virus disease 2019. PLoS ONE **15**, e0239960 (2020)
34. J.K.K. Asamoah, C.S. Bornaa, B. Seidu, Z. Jin, Mathematical analysis of the effects of controls on transmission dynamics of SARS-CoV-2. Alex. Eng. J. **59**(6), 5069–5078 (2020)
35. Q. Lin, S. Zhao, D. Gao, A conceptual model for the coronavirus disease, et al., (COVID-19) outbreak in Wuhan, China with individual reaction and governmental action. Int. J. Infect. Dis. **93**(2020), 211–216 (2019)
36. S.M. Kassa, J.B. Njagarah, Y.A. Terefe, Analysis of the mitigation strategies for COVID-19: from mathematical modelling perspective. Chaos Solitons Fractals **138**, 109968 (2020)
37. C. Anastassopoulou, L. Russo, A. Tsakris, C. Siettos, Data-based analysis, modelling and forecasting of the COVID-19 outbreak. PLoS ONE **15**, e0230405 (2020)
38. L. Lopez, Y. Rodo, A modified SEIR model to predict the COVID-19 outbreak in Spain and Italy: simulating control scenarios and multi-scale epidemics. Res. Phys. **21**, 103746 (2021)
39. A. Radulescu, C. Williams, K. Cavanagh, Management strategies in a SEIR-type model of COVID 19 community spread. Sci. Rep. **10**, 21256 (2020)
40. B. Ivorra, M.R. Ferrández, M. Vela-Pérez, A.M. Ramos, Mathematical modeling of the spread of the coronavirus disease 2019 (COVID-19) taking into account the undetected infections. The case of China, *Commun. Nonlinear Sci. Numer. Simul.***88**, 105303 (2020)
41. S. Zhao, Q. Lin, J. Ran et al., Preliminary estimation of the basic reproduction number of novel coronavirus (2019-nCoV) in China, from 2019 to 2020: a data-driven analysis in the early phase of the outbreak. Int. J. Infect. Dis. **92**, 214–217 (2020)
42. K. Liang, Mathematical model of infection kinetics and its analysis for COVID-19, SARS and MERS, Infection. Genet. Evol. **82**, 104306 (2020)
43. B. Tang, N.L. Bragazzi, Q. Li, S. Tang, Y. Yiao, J. Wu, An updated estimation of the risk of transmission of the novel coronavirus (2019-ncov). Infect. Dis. Model. **5**, 248–255 (2020)
44. H. Yiong, H. Yan, Simulating the infected population and spread-trend of 2019-ncov under different policy by eir model. Available at SSRN 3537083 (2020)
45. B. Tang, X. Wang, Q. Li, N.L. Bragazzi, S. Tang, Y. Xiao, J. Wu, Estimation of the transmission risk of the 2019-nCoV and its implication for public health interventions. J. Clin. Med. **9**(2), 462 (2020)
46. F.B. Hamzah, C. Lau, H. Nazri, D.V. Ligot, G. Lee, C.L. Tan, M.H. Chung, CoronaTracker: worldwide COVID-19 outbreak data analysis and prediction. Bull. World Health Organ. **1**(32), 1–32 (2020)
47. S.J. Clifford, P. Klepac, K. Van Zandvoort, B.J. Quilty, R.M. Eggo, S. Flasche, et al.: Interventions targeting air travellers early in the pandemic may delay local outbreaks of sars-cov-2. medRxiv (2020)
48. Y.M. Chu, R. Zarin, A. Khan, S. Murtaza, A vigorous study of fractional order mathematical model for SARS-CoV-2 epidemic with Mittag-Leffler kernel. Alex. Eng. J. **71**, 565–579 (2023). https://doi.org/10.1016/j.aej.2023.03.037
49. R. Zarin, U.W. Humphries, A robust study of dual variants of SARS-CoV-2 using a reaction-diffusion mathematical model with real data from the USA. Eur. Phys. J. Plus **138** (2023). https://doi.org/10.1140/epjp/s13360-023-04631-9
50. A. Omame, A.A. Raezah, G.A. Okeke et al., Assessing the impact of intervention measures in a mathematical model for monkeypox and COVID-19 co-dynamics in a high-risk population. Model. Earth Syst. Environ. **10**, 6341–6355 (2024). https://doi.org/10.1007/s40808-024-02132-x
51. G. Rohith, K.B. Devika, Dynamics and control of COVID-19 pandemic with nonlinear incidence rates. Nonlinear Dyn. **101**(3), 2013–2026 (2020)
52. J. Huang, G. Qi, Effects of control measures on the dynamics of COVID-19 and double-peak behavior in Spain. Nonlinear Dyn. **101**(3), 1889–1899 (2020)
53. C.J. Silva, C. Cruz, D.F.M. Torres, A.P. Munuzuri, A. Carballosa, I. Area, J.J. Nieto et al., Optimal control of the COVID-19 pandemic: controlled sanitary deconfinement in Portugal. Sci. Rep. **11**, 3451 (2021)
54. F. Brauer, *Compartmental models in epidemiology* (Berlin, Heidelberg, Mathematical epidemiology. Springer, 2008), pp.19–79
55. R. Niu, E.W. Wong, Y.C. Chan, M.A. Van Wyk, G. Chen, Modeling the COVID-19 pandemic using an SEIHR model with human migration. IEEE Access **8**, 195503–195514 (2020)
56. S. S. Dragomir, and M. City, Some Gronwall type inequalities and applications, (2002) URL: https://ssrn.com/abstract=3158353
57. O.N. Bjørnstad, *Epidemics: Models and Data Using R* (Springer-Verlag, New York, 2018)
58. J. Ma, D.J. Earn, Generality of the final size formula for an epidemic of a newly invading infectious disease. Bull. Math. Biol. **68**, 679–702 (2006)
59. J.C. Miller, A note on the derivation of epidemic final sizes. Bull. Math. Biol. **74**, 2125–2141 (2012)
60. P. Van den Driessche, J. Watmough, Reproduction numbers and sub-threshold endemic equilibria for compartmental models of disease transmission. Math. Biosci. **180**(1–2), 29–48 (2002)
61. P. Van den Driessche, J. Watmough, Further notes on the basic reproduction number. Math. Epidemiol., 159–178 (2008)
62. O. Diekmann, J.A.P. Heesterbeek, J.A. Metz, On the definition and the computation of the basic reproduction ratio R_0 in models for infectious diseases in heterogeneous populations. J. Math. Biol. **28**(4), 365–382 (1990)

63. E. Routh, A Treatise on the Stability of a Given State of Motion: Particularly Steady Motion. Being the Essay to which the Adams Prize was Adjudged in 1877, in the University of Cambridge. Macmillan and Company, 1877
64. J.W. Rogers, Locations of roots of polynomials. SIAM Rev. **25**(3), 327–342 (1983)
65. A. Hurwitz, On the conditions under which an equation has only roots with negative real parts. Selected papers on mathematical trends in control theory **65**, 273–284 (1964)
66. J.P. LaSalle, *The Stability of Dynamical Systems*, Society for Industrial and Applied Mathematics, (1976)
67. J.P. LaSalle, Some Extensions of Liapunov's Second Method. IRE Transactions on Circuit Theory **7**(4), 520–527 (1960). https://doi.org/10.1109/TCT.1960.1086720
68. J.K. Hale, S.M.V. Lunel, *Introduction to functional differential equations*, vol. 99 (Springer Science & Business Media, 2013)
69. J. K. Hale, Functional differential equations. In Analytic theory of differential equations, 9–22. Springer, Berlin, Heidelberg (1971)
70. W. H. Fleming, R. W. Rishel, *Deterministic and stochastic optimal control*, vol. 1. (Springer Science & Business Media, 2012)
71. D.L. Lukes, *Differential equations: classical to controlled* (Academic Press, New York, 1982)
72. L.S. Pontryagin, *Mathematical theory of optimal processes* (CRC Press, 1987)
73. M.I. Kamien, N.L. Schwartz, *Dynamic optimization: the calculus of variations and optimal control in economics and management* (Elsevier Science B.V, North-Holland, 2012)

Publisher's Note Springer Nature remains neutral with regard to jurisdictional claims in published maps and institutional affiliations.